A VARYING FIELD SIZE TRANSLATIONAL BED TECHNIQUE FOR TOTAL BODY IRRADIATION.

By Ben Wilder.

A thesis submitted for the degree of
Master of Science in Medical Physics
at the University of Canterbury, Christchurch,
New Zealand.

August 2006

CONTENTS

Contents

ABSTRACT.

Total body irradiation is the irradiation of the entire patient as a conditioning for bone marrow transplants. The conditioning process involves destroying the bone marrow allowing for repopulation of the donor bone marrow cells, suppression of the immune system to allow stop graft rejection, and to eliminate the cancer cell population within the patient. Studies have been done demonstrating the importance of TBI conditioning for BMT[5].

A range of TBI treatment techniques exist, this department uses a bi-lateral technique which requires bolus packed around the patient to simplify the geometry of the treatment. This investigation will focus on one technique which involves using a translating bed. This technique effectively scans a radiation beam over the patient as the bed moves through the beam. Other investigations on translating beds concentrated on varying the scan speed to achieve a dose uniformity to within ±5%. The recommendations quote a dose uniformity of +5% and -10% as acceptable[9]. The dose uniformity in these investigations was along the midline in the longitudinal direction only. This investigation varied field size to achieve dose uniformity to within ±2.5% along the midline of an anthropomorphic phantom. The goal was to determine if a dynamic multi-leaf collimator could be used to give a uniform in the transverse direction as well as the longitudinal direction. An advantage of utilizing the DMLC for this treatment is the ability to shield organs at risk, i.e. lungs and kidneys, without requiring resources to produce shielding blocks[14]. Gafchromic-EBT film[18] was used as a dosimeter but gave unreliable results due to the lack of film scanning equipment with an appropriate sensitivity for reading the dose to the film.

Scans were simulated using Xio treatment planning software. The results from the simulations gave a more reliable indication of the absorbed dose to the midline of the phantom. The disadvantage of this varying field size technique was the time and complexity involved in creating a treatment plan. Within the Xio software exists a limit on the number of beams allowed to be applied in a single plan. There is a maximum of 99 beams allowed which is not enough for complete coverage of a patient. A way around this is to increase the field sizes and decrease the scan speed. This option was not investigated. The advantage of this technique was the increased dose uniformity (±2.5%) in comparison to the varying scan speed techniques (±5%).

This technique also allows the patient to be unencumbered during the treatment making the process more comfortable for them.

ACKNOWLEDGEMENTS.

I would like to acknowledge the Christchurch Hospital, Medical Physics and Bioengineering Department and the Oncology Department for providing the equipment, alterations to the equipment and allowing time on their linear accelerators. I would like to thank David Pinchin (Linac Engineer in the Oncology Department) for the scanning bed program and the interfacing with the controller computer and the scanning bed, and Deloar Hossain for his selfless support and helpful discussion. I would also like to thank Mark Bird, my university supervisor Lou Reinisch and my clinical tutor John Turner for the proof-reading of my thesis. In the early stages of the development of my thesis I am greatly appreciative of the help from my supervisor Wen-Long Hsieh and John Turner.

LISTS OF FIGURES AND TABLES.

Page Figures

Page Tables

1. INTRODUCTION

Total body irradiation (TBI) has been used since the 1930's for treating leukemia patients[1]. The first published description[2] of a dedicated TBI in North America described a caged canary being used to determine when the treatment should end. The death of the canary was the signal for the treatment to stop. Nowadays TBI is a lot safer.

The conditioning of BMT using TBI has become a standard procedure for the treatment of a range blood disorders including leukemia[3, 4]. A study done by Inoue T, et al[5] in 1993 comparing allogeneic BMT for acute leukemia with TBI conditioning and without TBI conditioning, demonstrated the importance of TBI conditioning for treating leukemia. The results of this study showed that two-year survivals were 77% and 51% for the group with TBI conditioning and without TBI conditioning respectively. Relapses and organ failure after two years were also lower for the group which used TBI conditioning in their treatments. The roles of TBI in treating leukemia are; to destroy the bone marrow, which allows for the repopulation of the donor bone marrow cells, to suppress the immune system, which prevents graft rejection, and to eliminate the cancer cell population within the patient. While a goal of TBI is to minimize toxicity while maximising anti-tumor and immunosuppressive effects[6]. Studies have been done which look at the application of TBI conditioning[6-8]. These studies look at the effects of total dose, dose fractionation, dose-rate and dose distribution have with regard to cancer cell kill rate and normal tissue toxicity. The results showed that increasing total dose and dose-rate achieved better immunosuppression but increased the toxicity, whereas fractionation achieved less immunosuppression, but decreased the toxicity effects. The ratio of cell killing to normal tissue toxicity is called the therapeutic ratio[8]. Conforming dose was discussed in these studies as an idea of focusing higher doses to smaller specific areas, i.e, bone marrow, lymphatic system, and avoiding sensitive areas by shielding, i.e. lungs, normal tissue. There exist a number of methods for shielding specific areas in TBI treatments. A more novel method of shielding is to use a multi-leaf collimator (MLC) or a dynamic multi-leaf collimator (DMLC). With the development of new TBI

techniques it is a hope that improved survival rates for patients requiring bone marrow transplants is improved.

The majority of TBI patients in the Christchurch Hospital Oncology Department are being treated for acute myeloid leukemia, acute lymphoblastic leukemia or chronic myeloid leukemia. The present technique within this department is a bi-lateral field technique. A specially designed TBI bed is used for the comfort of the patient. Two perspex walls are placed on either side of the patient and held in place by perspex 'combs'. Sterilized rice bags are then placed around the patient to compensate for the contour variations and achieve better dose uniformity (within ±5%). The gantry is rotated to 90˚ and the collimator is rotated to 45˚. Rotating the collimator 45˚ allows the length of the patient to fit within the treatment beam. Diagonal profiles are taken every six weeks during QA tests to measure the off-axis variation so it can be taken into account when prescribing the dose along the midline. This is due to the flattening filters only being designed to achieve flatness along the two principle planes and not the diagonal plane[9]. The patient and TBI couch are positioned on the far side of the room to give a field as large as possible. In this technique setup time is an issue. It is also difficult for the patient having rice bags placed around, if there is an emergency, e.g. the patient becomes nauseous and needs to vomit, they would need to be able remove the bags[1] and sit up relatively quickly.

The setup with a bi-lateral field technique has the beams traveling through a large distance of tissue. This causes a variance in uniformity which is greater in comparison to an anterior-posterior/posterior-anterior (AP/PA) technique which has beams traveling through less tissue. The recommendation for dose uniformity in TBI treatment techniques is between +5% and -10%[9, 10]. A disadvantage with an AP/PA technique in a clinical setup is the limitations on the field size due to the rooms' size. The distance from the source to the floor is not large enough to achieve a beam which will cover the whole body. This limitation could be overcome by a technique using an Arc-TBI[1], this is where the gantry is rotated through an angle and effectively scanning the radiation beam over the patient. This study achieved better overall dose uniformity (the exception being in the neck and supraclavicular regions, 6.6%) in comparison with the current technique.

Two papers have been summarised which relate to a translating bed technique. The first technique described in chapter 2 involves a translating couch where the machine dose-rate variation is compensated for by modulating the couch speed. The authors Mehrdad Sarfaraz et al introduce calculations for converting from a moving beam output to a fixed beam output factor. Calculations for determining the translating speed of the couch are also introduced. A comparison is made between the original TBI technique of using fixed AP/PA fields and the alternative technique of using a translating couch. Dose variation in the translating couch technique was from 100% at the hip and mid chest regions to 117% at the ankles and neck regions. This was slightly better than the fixed AP/PA technique. A speed modulated technique was suggested as a way of further increasing uniformity.

The second technique described in chapter 3 involved a translating couch where the speed variation was used to increase the dose uniformity to the midline of the patient. The authors Mario Chretien et al use a beam weighted method for determining the speed variation. An equation is introduced relating the couch speed to the beam weighting. The varying couch speed technique is compared to a constant couch speed technique. The aim was to achieve a dose uniformity of ±5% or better. Using a varying speed technique a dose variation of less than 4% was achieved.

In these two papers[11, 12] a beam spoiler was used to increase the skin dose to the patient. This investigation does not use a beam spoiler due to it not being necessary for the purpose of this experiment. This technique was also not clinically implemented, a beam spoiler would be required if the technique was to be used on patients to increase the skin dose. The techniques described by Mario Chre´ tien and Mehrdad Sarfaraz were clinically implemented and so a beam spoiler was used.

In this report a translating bed technique will be investigated, where the field size is varied as opposed to varying the bed speed. This technique uses AP/PA fields. The beam is effectively scanned over the patient as the TBI bed moves through the beam. Any variations in the beam itself will be spread out along the movement direction giving better dose uniformity, whereas in a fixed beam technique one point in the patient is always under one point in the beam profile[11]. Several papers have investigated a translating varying couch speed to modulate the beam[11, 12, 13]. Though they only deal with beam modulation in the longitudinal direction.

The initial concept was the use of a DMLC in modulating the beam to conform it to the contours of the body transversally and longitudinally in order to achieve a greater level of uniformity. A 21 iX Varian Linac was used. This concept would not be achievable in the time available. It was decided that the first step towards this concept would be investigated. The first step was to simulate a single leaf pair movement (using collimator jaws) along the central sagittal plane of an anthropomorphic phantom and determine the dose uniformity along this plane. The distance between the jaws (slit width) which would deliver the prescribed dose 100cGy was calculated and compared to measurements using Gafchromic-EBT film. Approximate alignment and leveling of the equipment made it difficult to obtain precise measurements for the scanning TMRs and slit width calculations.

2. SUMMARY OF A STUDY INVOLVING A TRANSLATIONAL COUCH TECHNIQUE FOR TOTAL BODY IRRADIATION.

2.1 INTRODUCTION

This chapter summarizes a study done by Mehrdad Sarfaraz et al[11], involving a TBI technique which utilizes a translating couch for TBI. This technique does not use couch speed modulation for compensating for the various thicknesses in a patient, but utilizes couch speed modulation for compensating for the machine dose-rate variation. The author Mehrdad Sarfaraz et al introduces calculations for converting from a moving beam output to a fixed beam output factor. Calculations for determining the translating speed of the couch were also introduced. A comparison was made between the original TBI technique of using AP/PA fixed fields and the alternative technique of using a translating couch.

2.2 METHOD AND MATERIALS.

2.2.1 Couch Design and Construction.

A steel frame, moving cradle and driving assembly make up the translating couch system. The cradle was moved along using a stepper motor to drive the conveyer belts. An indexer was used to move the cradle at a calculated speed. The dose to the patient was dependant on the couch speed assuming a constant machine dose-rate. The couch speed was updated continuously to compensate for any machine dose-rate fluctuations.

2.2.2 Treatment Setup.

This system scans a patient through a 6MV beam in the supine and prone positions. The source to couch distance was set at 160cm. 50cm of clearance from the floor allows backscatter to be reduced. A plexi-glass spoiler was hung from the collimator head to increase the surface dose to the skin. The translating couch system is shown below (*Mehrdad Sarfaraz et al*).

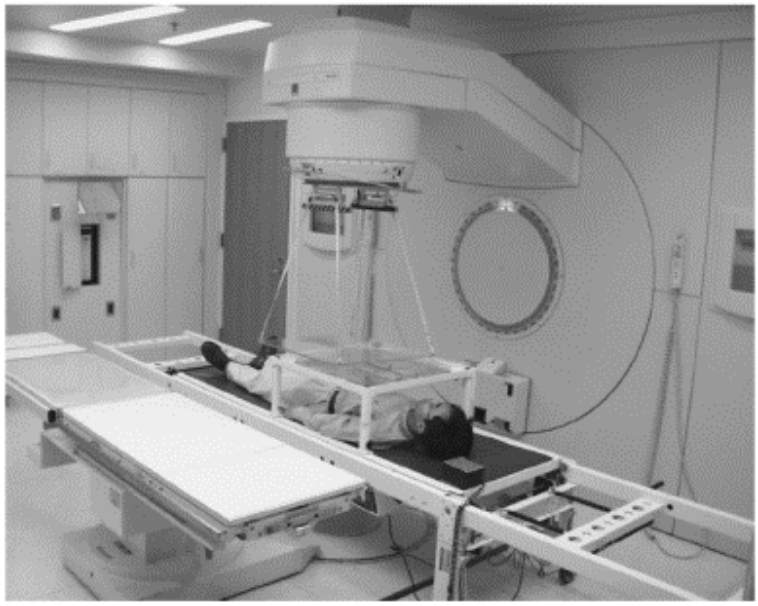

Fig 2.1. Translating couch equipment and setup used in this technique. The beam spoiler and cradle can be seen. Courtesy of Mehrdad Sarfaraz et al.

The dose was prescribed to the umbilicus at midline depth. Doses at other body sections were also recorded. Simulating the patient gave the SSD and thickness at several points for supine and prone positions. These parameters plus the prescribed dose, field length and machine dose-rate were entered into the computer for calculating the couch speed.

2.2.3 Dosimetry.

Tissue maximum ratios (TMRs) were measured directly for the specific TBI setup. These TMRs were different from standard TMRs due to the scanning process. They were referred to as moving TMRs and were measured in a 40 x 30 x 30cm water tank.

2.3 THEORY

2.3.1 Dose Calculations.

As the patient translates through the beam a point within the patient will receive a dose equal to the area under the beam profile in the longitudinal direction.

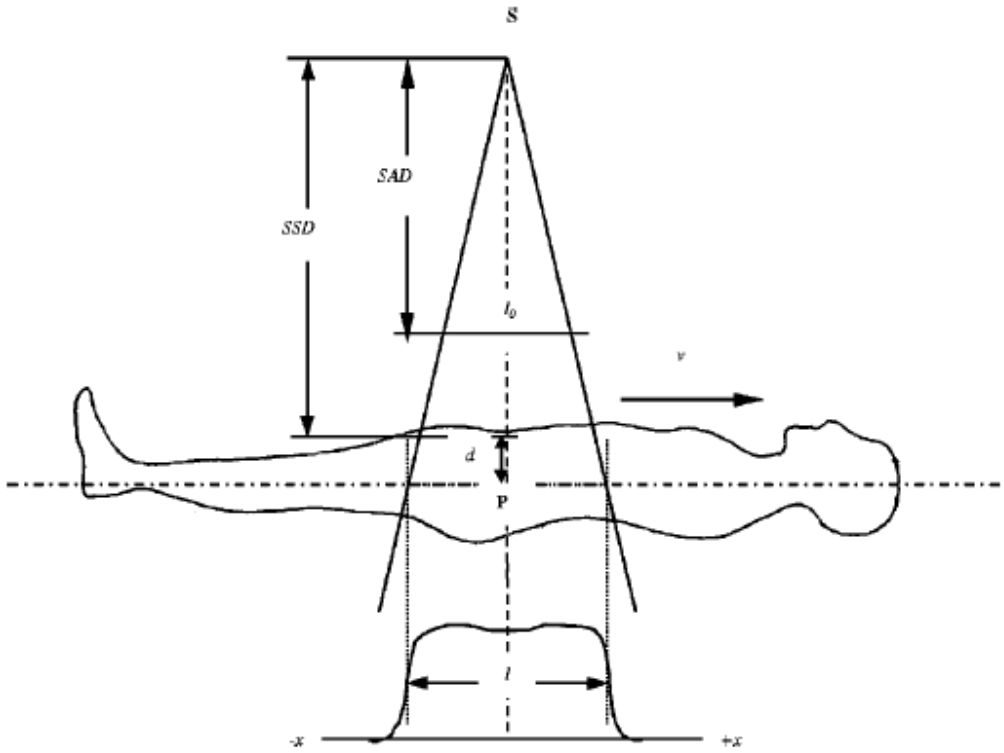

Fig 2.2. Physical situation used to derive the dose calculations. Courtesy of Mehrdad Sarfaraz et al.

The area under the beam profile can be found by integrating the instantaneous dose-rate over time. The beam profile curve was described by the equation below.

$$\dot{D}(d,x,r) = \dot{D}_{CAX}(d,r) \times OAR(d,x,l), \tag{1}$$

Where D_{CAX} and OAR are the central axis dose-rate and the Off-axis-ratio respectively, d is the depth to point P lying on the midline, r is the equivalent field size with width w and length l.

Integrating the beam profile curve,

$$D(d,r)=\int_{-\infty}^{+\infty}\dot{D}(d,x,r)dt=\int_{-\infty}^{+\infty}\dot{D}_{CAX}(d,r)\times OAR(d,x,l)dt. \quad (2)$$

Since $dt = dx/v$, dx/v is substituted for dt giving the equation below.

$$D(d,r)=\dot{D}_{CAX}(d,r)\times\frac{1}{v}\times\int_{-\infty}^{+\infty}OAR(d,x,l)dx. \quad (3)$$

The *moving TMR* was given by,

$$TMR_{moving}(d,r)=\frac{D(d,r)}{D(d_{\max},r)}=\frac{\dot{D}_{CAX}(d,r)\times\int_{-\infty}^{+\infty}OAR(d,x,l)dx}{\dot{D}_{CAX}(d_{\max},r)\times\int_{-\infty}^{+\infty}OAR(d_{\max},x,l)dx} \quad (4)$$

By this theory the *fixed TMR* was corrected by the ratio of the integrated *OARs* at d and d_{max} to give the *moving TMRs*..

$$TMR_{moving}(d,r)=TMR_{fixed}(d,r)\times\frac{\int_{-\infty}^{+\infty}OAR(d,x,l)dx}{\int_{-\infty}^{+\infty}OAR(d_{\max},x,l)dx} \quad (5)$$

From the dose at d_{max} the dose to point P can be calculated using the *moving TMR* values.

$$D(d,r)=D(d_{\max},r)\times TMR_{moving}(d,r). \quad (6)$$

2.3.2 Couch Velocity Calculations.

Expanding equation (6) using equation (3) gave,

$$D(d,r) = \dot{D}_{CAX}(d_{\max},r) \times TMR_{moving}(d,r) \times \frac{1}{v} \times \int_{-\infty}^{+\infty} OAR(d_{\max},x,l)dx, \quad (7)$$

The dose on the central axis at depth d_{max} at extended SSD was derived from

$$\dot{D}_{CAX}(d_{\max},r) = \dot{M} \times D_0 \times S_{c,p} \times TF \times \left(\frac{100}{SSD+d}\right)^2. \quad (8)$$

Where *Sc,p* is the field size output factor at extended SSD, *TF* is the tray spoiler factor, *M* the machine dose-rate at the iso-center, D_0 the reference calibrated dose at the iso-center and at d_{max}.

With the *m* factor defined as,

$$m = \frac{\int_{-\infty}^{+\infty} OAR(d_{\max},x,l)}{l} \quad (9)$$

where,

$$l = l_0 \times \left(\frac{SSD+d}{100}\right),$$

The dose to point P, using equations (7) to (9) was expressed as,

$$D(d,r) = \dot{M} \times D_0 \times TMR_{moving}(d,r) \times S_{c,p} \times TF \times \frac{m \times l_0}{v} \times \left(\frac{100}{SSD+d}\right). \quad (10)$$

Rearranging equation (10) gave,

$$v = \frac{\dot{M} \times D_0 \times TMR_{moving}(d,r) \times S_{c,p} \times TF \times m \times l_0 \times (100/SSD+d)}{PD} \quad (11)$$

Where *PD* is the prescribed dose at depth *d* for the field size *r*.

2.4 RESULTS

2.4.1 Moving and Fixed TMRs.

Mehrdad Sarfaraz et al found that their moving TMRs were equivalent to the fixed TMRs but suggested further independent investigations be done to confirm these results as they may differ between machines and departments.

2.4.2 Output Factors.

The factor that converts the moving beam output to a fixed beam output for the same setup is the *m* factor. The *m* factor had been defined as the moving beam output factor, and was considered as the ratio of the area under the actual beam profile to the area under an idealized beam profile. The ratio can be calculated from Equation (9) or measured as the ratio of the integral dose with the moving beam divided by the stationary beam central axis dose for the same setup.

2.4.3 Shielding Block.

Cerrobend blocks were place on the plastic cover of the moving cradle to shield organs at risk (Fig 2.1). It was found that points under the shielding block still received a dose. This effect was compared to stationary shielding (Fig 2.5).

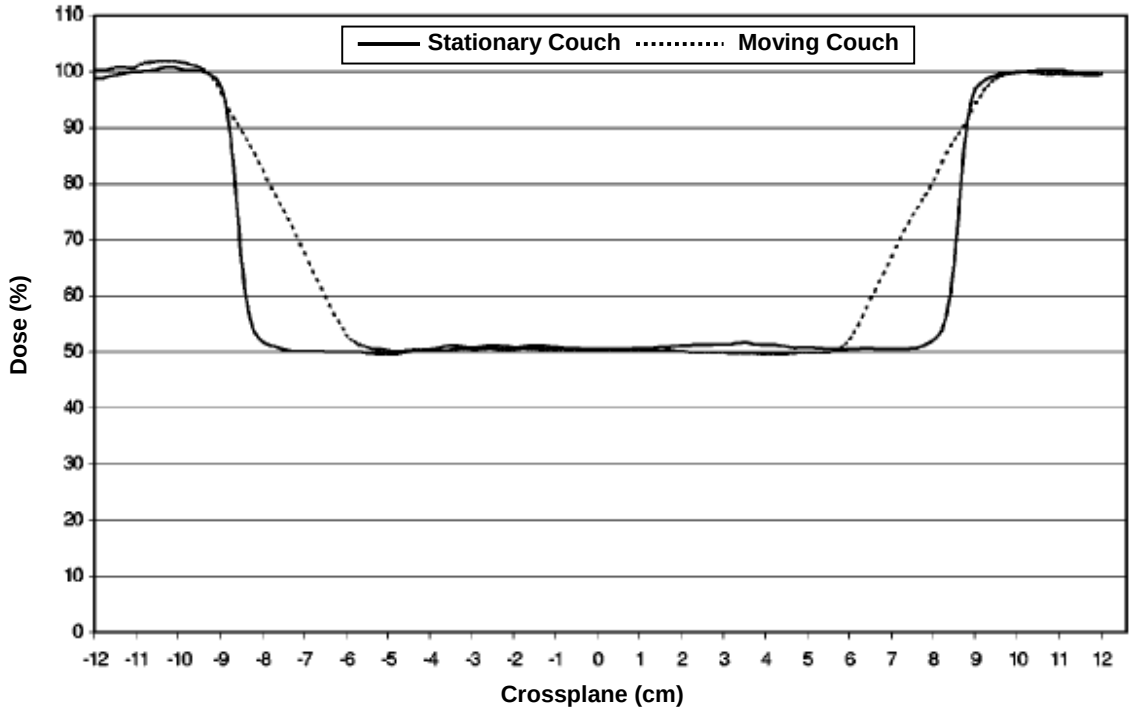

Fig 2.3. The solid line represents the shielding from a stationery couch, the dotted line represents the shielding from a moving couch. Courtesy of Mehrdad Sarfaraz et al.

As the shielding moves up to and through the radiation beam the diverging beam is able to irradiate an area under the shielding. This also occurs when the shielding passes out of the beam. This is illustrated in Fig 2.4.

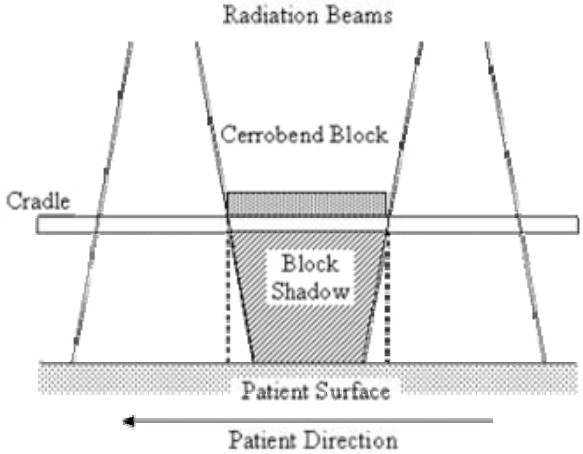

Fig 2.4. This diagram illustrates the shielding under a block of cerrobend with a translating couch technique. The dotted line represents the shadow cast by a cerrobend block with a stationary couch technique.

This effect could be reduced by decreasing the distance the shielding was from the skin or decreasing field width.

2.4.4 Dose Verification.

A dose of 125cGy was prescribed to the mid plane, 62.5cGy to the right lung. TLDs were placed inside an anthropomorphic phantom at various positions along the mid plane (Fig 2.5). TLDs were also positioned in the left and right lung, the right lung was partially shielded. The measurements were compared to the calculations, an agreement of better than 3% was found for all positions except the forehead and right lung.

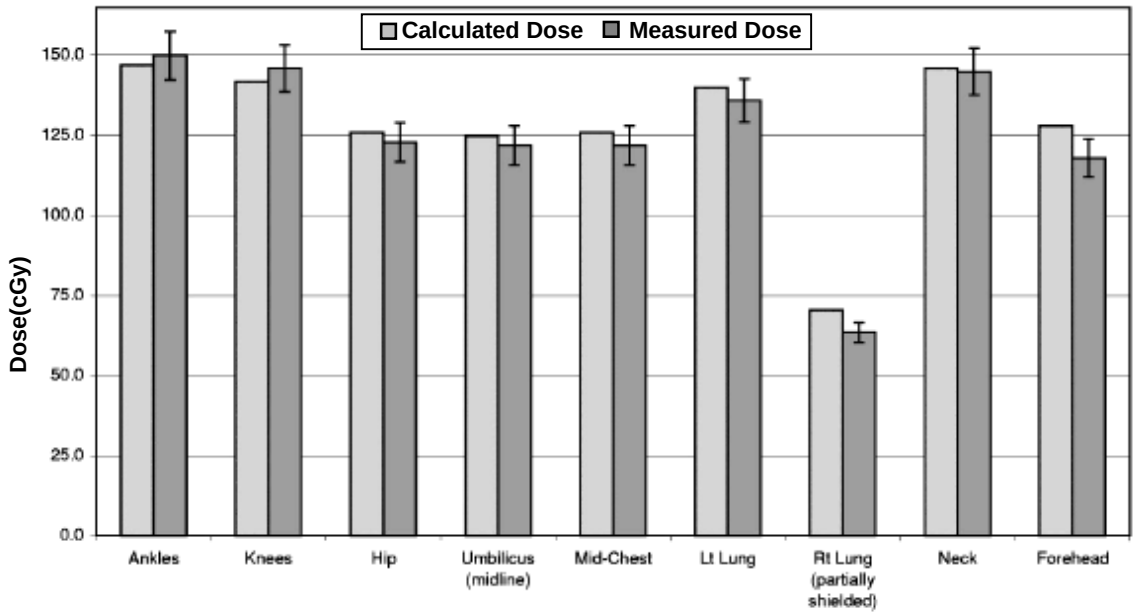

Fig 2.5. Comparison of measured dose (dark gray bars) and calculated dose (light gray bars) at various positions along the midplane.

The dose variations were compared to the dose variations using a stationary beam technique. The moving beam technique showed a slightly better uniformity than the stationary beam technique (Fig 2.6).

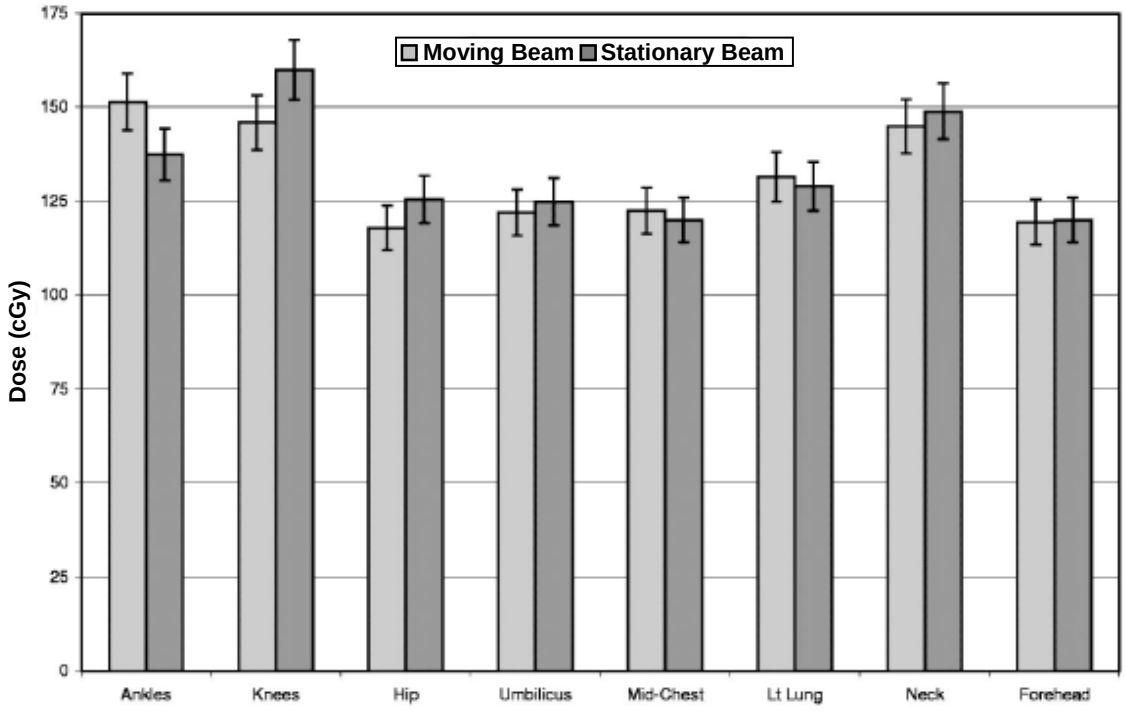

Fig 2.6. Comparison between moving beam technique (light gray bars) and the stationary beam technique (dark gray bars).

2.5 DISCUSSION.

This technique achieved increased dose uniformity through the patient in comparison to the fixed field technique. The treatment time was 20 minutes per beam which was twice the treatment time for a fixed beam technique. The authors were investigating a way to increase the dose-rate within the patient to reduce this treatment time. Over most regions the measured versus calculated doses were within 3%. It was suggested that increased uniformity could be achieved by modulating the couch speed to compensate for the varying thickness of the patient. A number of studies have investigated couch speed modulation for a translational couch TBI treatment technique[12, 13].

3. SUMMARY OF A STUDY INVOLVING A VARIABLE SPEED TRANSLATING COUCH TECHNIQUE FOR TOTAL BODY IRRADIATION.

3.1 INTRODUCTION

This chapter summarizes a study done by Mario Chretien et al[12] which utilizes a translating couch where the speed modulation was used to increase the dose uniformity to the midline of the patient by compensating for the patient thickness variation. The authors Mario Chretien et al use a beam weighted method for determining the speed variation. An equation was introduced relating the couch speed to the beam weighting. The varying couch speed technique was compared to a constant couch speed technique. The aim was to achieve a dose uniformity of ±5% or greater.

3.2 METHOD AND MATERIALS.

3.2.1 Moving Couch.

The variable speed couch sits on a rail system on the floor of the treatment room. A computer drives a stepper motor which drives the couch assembly. The couch speed was varied using the computer via an indexer. The rails were long enough to accommodate a tall patient. The full scan length, where the patient started outside the beam and ended outside the beam, was about 4 meters. A remote controlled translation system can control the speed and position of the couch.

3.2.2 Technical Aspects.

Experimental measurements were made with an ionization chamber. TMR, PDD, scattering factor, beam spoiler and attenuator measurements were done at 214cm source couch distance. Static and dynamic modes were used to collect data for commissioning of technique and dose planning. A beam spoiler was used to increase skin dose, and was mounted onto the linac. The beam spoiler was acrylic plastic,

1.3cm thick and was 10-15cm above the highest point of the patient. For protection of organs at risk i.e, lungs, kidneys or liver, lead attenuators were used.

3.2.3 Simulation and CT Scans.

During simulation cushions and other accessories were used to keep the patient comfortable while they were being irradiated. The shapes of the attenuators were determined during the simulation time. Film was used to acquire an image of the organ and the shape was defined from the image.

3.3 IMRT DOSE PLANNING.

3.3.1 Beam Weight Optimization.

The planning dosimetry required a large number of beams distributed over the body. Up to 72 beams were used with an approximate 2cm shift between each beam as shown in Fig 3.1. Each shift was calculated using field length, patient length and the number of beams. Each beam was 60cm wide and 30cm long at the mid plane. Dose points were created on each CT slice and the dose contribution from each beam with and a beam weight of one was computed. Theraplanplus from MDS Nordion was the treatment planning software used to generate the beams and perform the dose calculations.

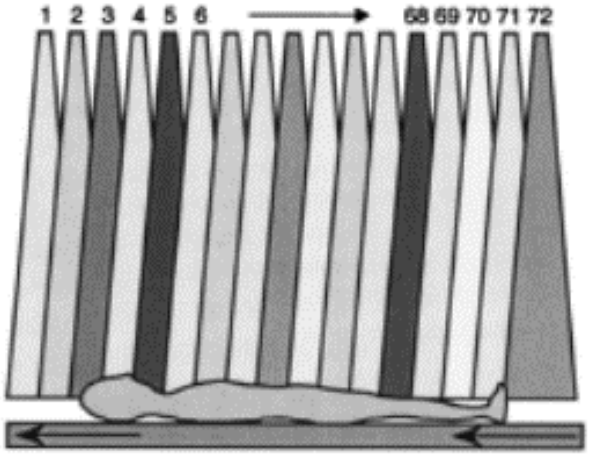

Fig 3.1. Diagram showing the 72 beams applied to the patient. Courtesy of Mario Chretien, et al.

3.3.2 Velocity Distribution.

Beam weights were proportional to the inverse of the scan velocity. A low speed increases the dose to a point within the patient. A higher speed reduces the dose to a point within the patient. The relationship is shown in the equation below, where V_i is the speed of beam number i, W_i is the beam weight of beam number i, and V_{ref} is the reference speed.

$$V_i = V_{\text{ref}} / W_i$$

The reference speed is the speed required to deliver the prescribed dose to a reference point, usually taken at the umbilicus.

3.4 RESULTS.

An ionisation chamber was used to measure the dose at five locations within an anthropomorphic phantom specially designed for this purpose. Dose measurements were done with a constant couch speed and then a varying couch speed and compared to the computations made by the TheraplanPLUS software.

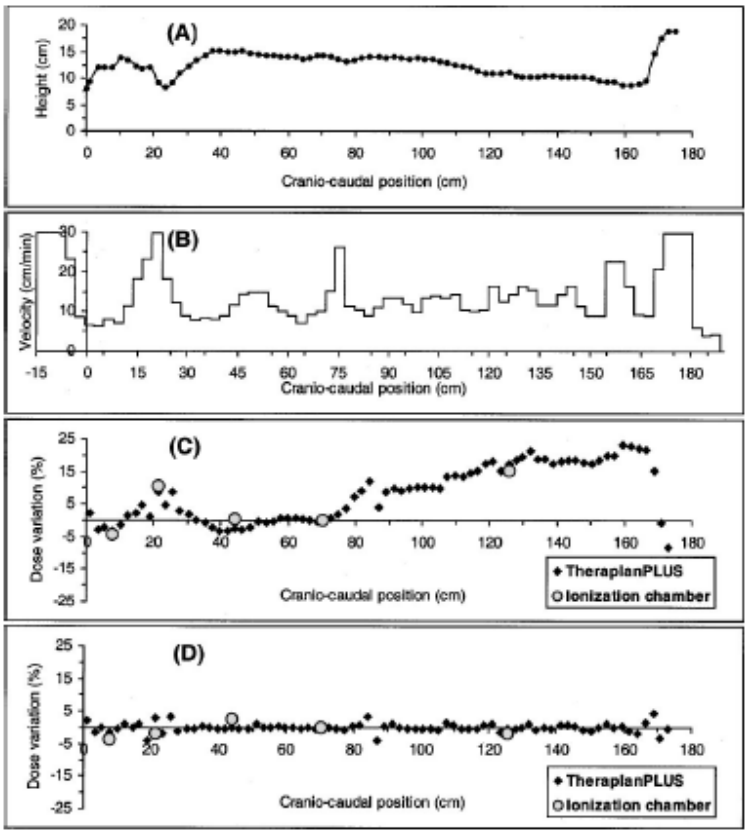

Fig 3.2. Diagram (A) illustrates the phantom profile, (B) illustrates the computed speed variation, (C) illustrates the dose variation with a constant couch speed, and (D) illustrates the dose distribution with a varying couch speed. Courtesy of Mario Chretien, et al.

The constant speed V_{ref} used in Fig 3.2C was 11.9cm/min. Doses in the neck and leg regions were up to 20% higher than the prescribed dose. With the speed distribution applied the resulting dose distribution shows a variation of less than 4% with an average deviation of 0.8% and a standard deviation of 1.3%.

3.5 DISCUSSION.

In this paper the technique investigated was developed and used on patients. The patient lies on the moving couch comfortably and the treatment time was 15min per incident beam. The treatment planning involved in the computation of the speed

distribution requires extra work compared to the more straight forward technique using a constant speed. The results however show a very good uniform dose distribution at the mid plane of the phantom.

4. EQUIPMENT.

4.1 INTRODUCTION.

The purpose of this chapter is to list and describe the equipment used in this report. Setup of equipment is described in the method and materials section.

The scanning bed shown in Fig 4.1 and 4.2 is a decommissioned GE gamma camera scanning bed acquired from the Nuclear Medicine department. Various modifications were made to the bed and are detailed in this chapter. The bed has a scan distance of 3 meters. The speeds were programmed using the controller computer.

The Varian 21 iX linac was recently installed and commissioned. One of its features was the DMLC. The DMLC was required in this report as it allowed for MLC movement while irradiating.

The Diagnostic Radiology Vidar scanner was the scanner used for scanning the irradiated Gafchromic film squares as the VXR-16 scanner was not working to specifications. Problems with the VXR-16 scanner are described in section 6.1.9. Images from the vidar scanner could then be analysed and dose measurements could be determined.

4.2 SCANNING BED SYSTEM.

4.2.1 System Components.

The scanning bed system consists of rails which were placed on the floor, a bed component which runs along the rails and the controller computer.

The rails are split into two sections. The main section consists of the worm drive screw on the left side (right side in Fig 4.1) and a guide slot on the right. This section was where the scanning bed travels. The second section of the rails was attached to the end of the main section and has the stepper motor, controller board and power supply attached (Fig 4.3). The stepper motor drives the screw which moves the bed along the rails. The controller board is connected to a cable which leads out of the treatment room and into the controller computer (Fig 4.4). A

schematic of this setup is illustrated in Fig 4.5. The cable was able to pass through a hole in the wall of the treatment room designed for the purpose of passing cables between the treatment room and the console area. The gamma bed required MDF board in order to create a flat surface for the phantom to sit on, as shown in Fig 4.1 and Fig 4.2.

Fig 4.1. Scanning bed on the main rails with the 21 iX Linac.

Fig 4.2. Scanning bed sitting on the rails. The left side of the rails has the screw and the right side has the guide slot.

Fig 4.3. Controller board, stepper motor and power Supply attached to the end section of the rails.

Fig 4.4. Scanning Bed Controller Computer. Behind the computer are cables which have been fed into the treatment room via a hole in the wall. The hole goes diagonally downwards to minimize scatter back through.

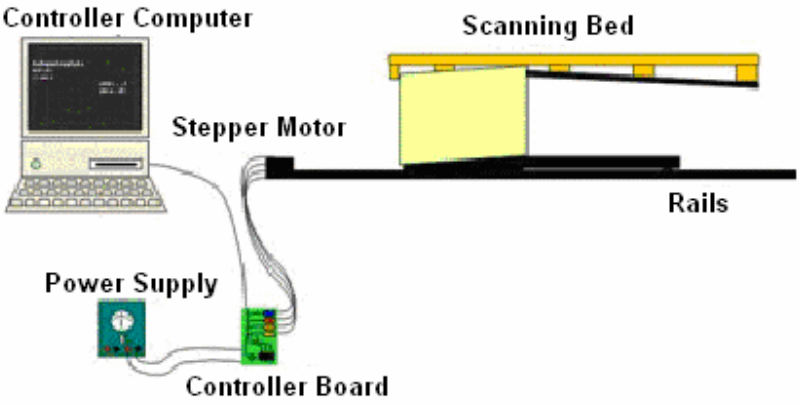

Fig 4.5. Basic schematic of the setup of the scanning bed system. Shown are the controller computer, power supply, controller board, stepper motor, rails and the scanning bed.

4.2.2 Modifications.

The scanning bed required modifications. The gamma camera bed was originally designed for a person to lie comfortably on the bed while it scanned through the gamma cameras. This meant that the bed itself was not flat and level along its length. A medium density fiber board was used to create a flat and level surface for the rectangular phantom to be placed on. This modification can be seen in the schematic shown in Fig 4.5.

Transporting the equipment to the treatment room was initially difficult. Wheels were made and attached to the rails and the scanning bed as shown in the Fig 4.6 below. This made transport of equipment to the treatment rooms easier and faster. Ramps were made allowing the scanning bed to be wheeled and lowered onto the rails. Fig 4.7 shows a schematic of the ramps and their setup.

The original controller board did not come with the gamma camera bed and rails. A substitute controller board was found and connected to the stepper motor.

A dedicated controller computer was connected to the controller board via the printer port using a printer cable. A program was compiled so the speed and distance of movement could be controlled by the operator outside the treatment room. Speed and distance calibration measurements are detailed in the next section.

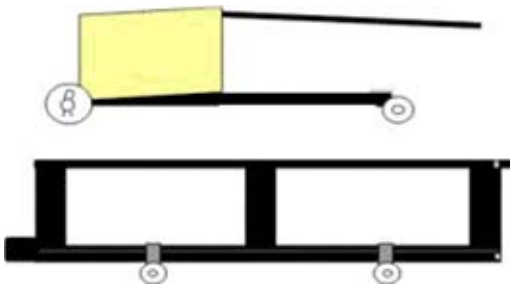

Fig 4.6. Position of wheel attachments on the scanning bed and rails.

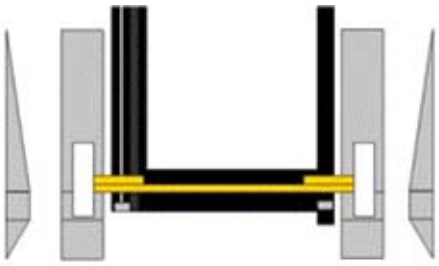

Fig 4.7. Wooden ramps were made to allow the bed to be set on the rails with no lifting.

4.2.3 Scanning Bed Calibration.

The scanning bed movement distance was calibrated by programming the bed to move 1 meter forwards then backwards to check for hysteresis. A metal ruler was used to measure the 1 meter distance along the rails. The rails were marked with the beginning and end positions of the scanning bed.

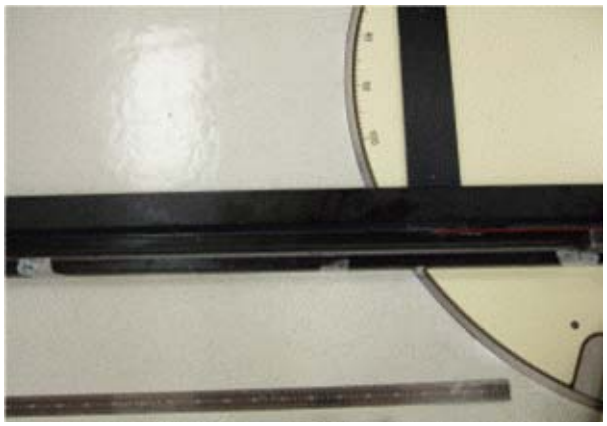

Fig 4.8. Scanning bed programmed distance calibration. A metal ruler is used to measure 1 meter. Beginning and end marks were made on the rails.

The controller computer initially required an input of a number of pulses to move the bed a certain distance. The distance a 1 pulse represented was determined by inputting a number of pulses then measuring the distance the bed moved. 1,000,000 pulses were entered into the controller computer and the scan distance measured. The scan distance was measured to be 2070mm. Pulses per millimeter equates to 483 pulses/mm, this represents approximately 2.1x10-3mm/pulse. The controller computer program was converted to read millimeters instead of pulses.

4.2.4 Scanning Bed Speed.

Bed speed was determined by the rate of pulses delivered to the stepper motor. The computer program had a continuous scale of speeds. Where the smaller the number the faster the scan speed. The maximum scan speed was dependant on the stepper motor. A range of speeds were timed to determine the speed in m/min. The measurements are shown in the Table 4.1 and graphed in Fig 4.9 below.

Scale	Speed (m/min)
0	1.053
1	0.833
2	0.706
4	0.541
6	0.375
12	0.273
16	0.219

Table 4.1. Scanning bed speeds in m/min for the speed scale on the controller computer.

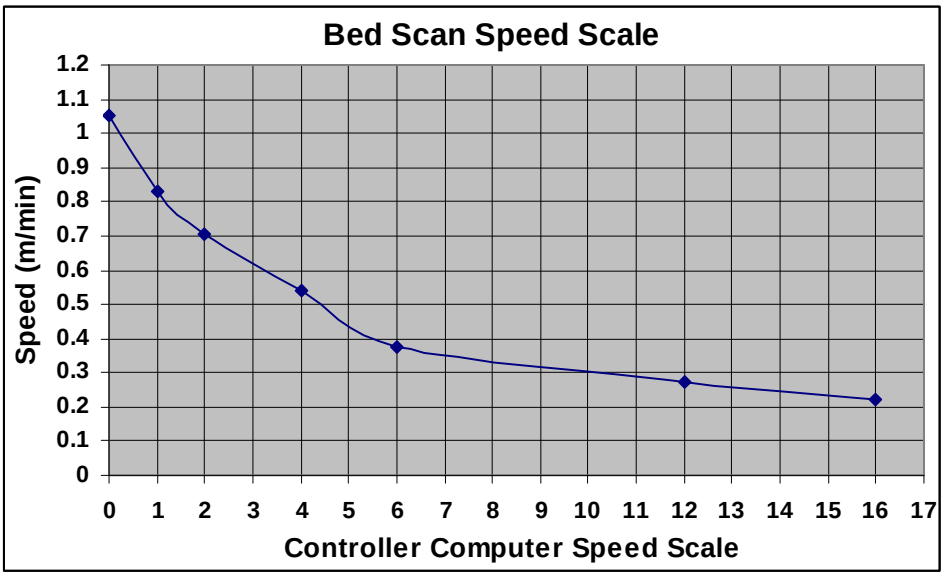

Fig 4.9. The Scanning Bed Control Computer Program has an integer speed scale. This graph shows the speeds (m/min) related to the computer program scale.

The bed speed used for all measurements in this report was chosen to be 2 on the speed scale which represents 0.706m/min. This allowed for the treatment time and

number of Monitor Units per scan to be calculated. This speed allowed a 3m scan to be completed in approximately 2 minutes.

4.2.5 Scanning Bed Program.

The program for controlling the translating bed was written by resident Linac engineer, Dave Pinchin, in Qbasic. The printed program file is shown in the appendix of this report. A diagrammatic version of the program can be seen below (Fig 4.10).

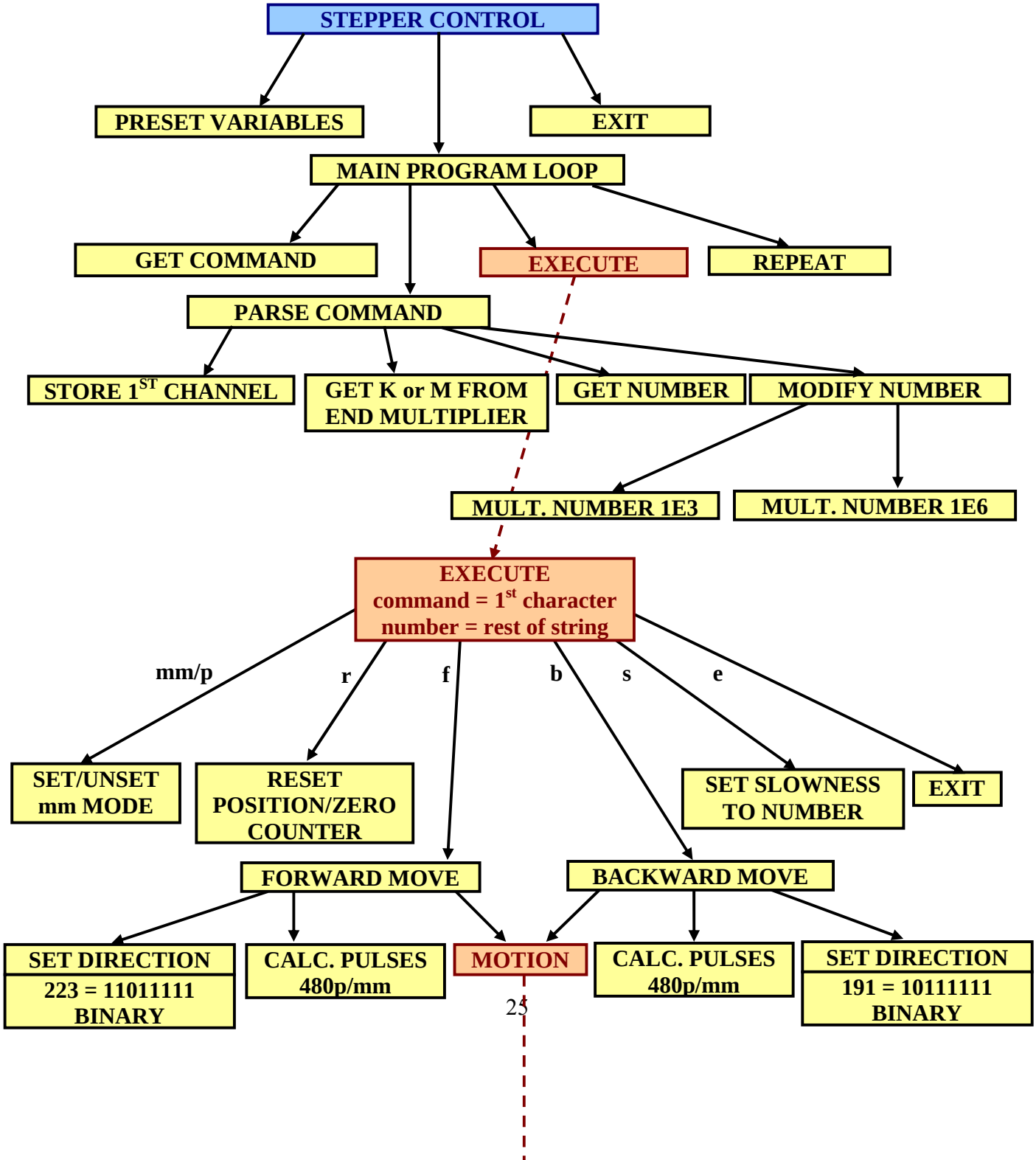

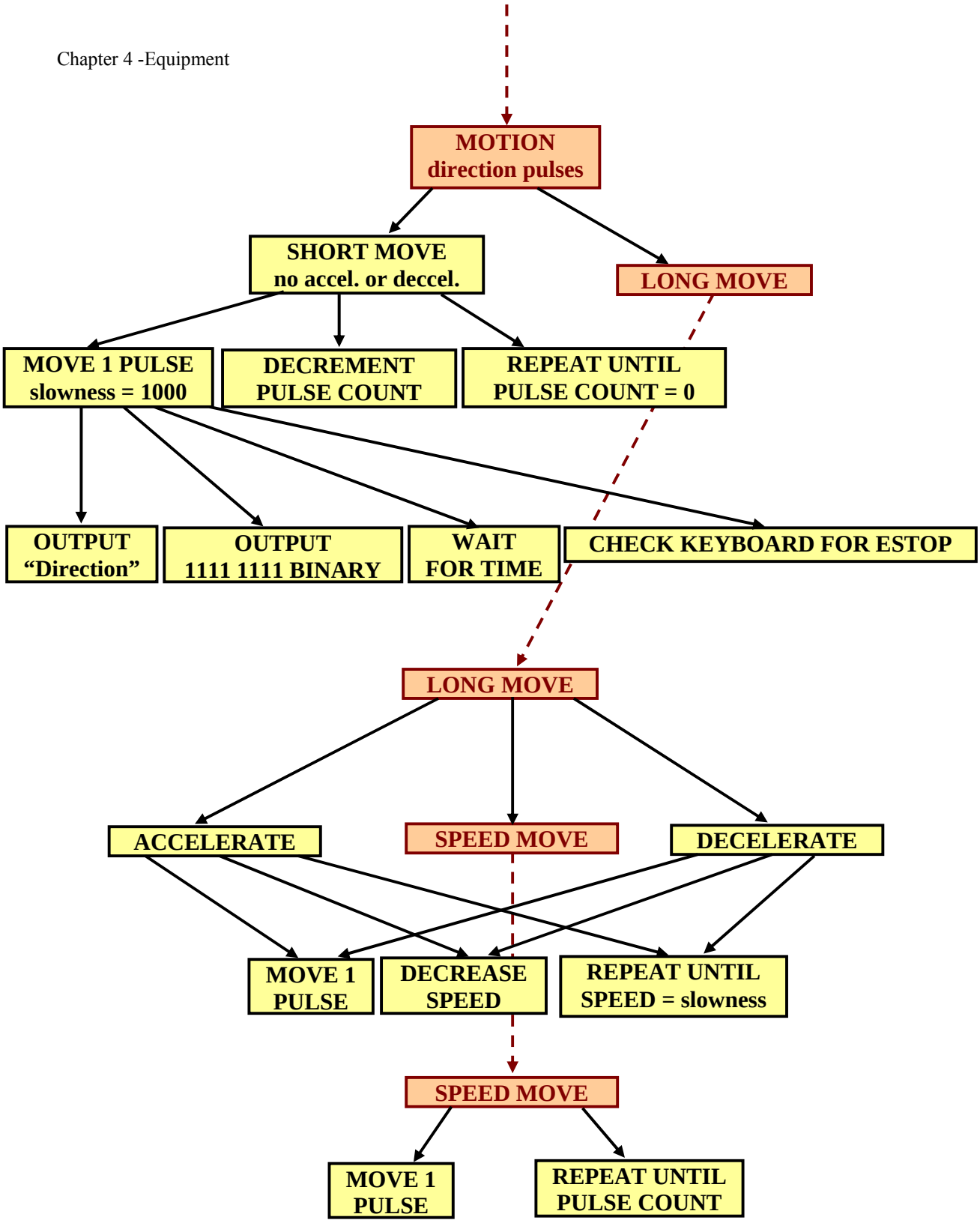

4.10. Program diagram showing the program paths. Printout of program file is found in the appendix.

4.3 VARIAN 21 IX LINEAR ACCELERATOR.

The 21 iX Linac was the latest model of Varian linacs and had been recently installed and commissioned. This linac was used because it was the only machine with a DMLC (120 leaves) within the department. The DMLC was used for measurements investigating the movement synchrony between the DMLC and the translating bed. The DMLC is described in the next section (4.4 Dynamic MLC).

Fig 4.11. 21 iX Varian Linear accelerator in the Christchurch Hospital Oncology Department.

4.3.1 Dynamic MLC[14].

The DMLC acts like physical compensators, though does not have the external beam modifier which modulates the beam intensity. The DMLC modulates the beam intensity by varying the position of the leaves while the linac is on. A DMLC involves significantly less overhead than physical compensators which are made for specific patients. They are also impractical for routine use in dose optimization because they increase the time for a treatment when different compensators need to be installed.
With DMLC nothing needs to be fabricated before or installed during the treatment. The dynamically compensated field is stored as an electronic file on the computer.

DMLCs are primarily useful for producing highly conformal 3D dose distributions. This allows dose escalation. Another advantage with DMLC is that there is no beam hardening effect and so the depth dose characteristics are more like open field depth dose characteristics.

A disadvantage of the DMLC is that programming the various fields becomes complex when a step increase or decrease in dose is required.

DMLC field files are downloaded to the Clinac-DMLC control system via ASCII text files.

4.4 DIAGNOSTIC RADIOLOGY VIDAR SCANNER.

This scanner had been specifically setup for diagnostic radiology work and included the ability to vary the windowing level (a constant window level was therefore chosen). The mode of scan was linear, the pixel values were equivalent to the bit size of the image (12-bit image, 4096 grey levels), as opposed to optical density (OD) used in the VXR-16 Vidar scanner, which gave pixel values equivalent to OD values (pixel value 10000 = 100% OD). The Software installed on the Diagnostic Radiology Vidar scanner was Agfa IMPAX TS5. To use this Vidar Diagnostic Radiology scanner a "patient" file was required to be set up. This involved inputting basic information (first and last name, NHI (National Health Index) number, current date, M/F). The NHI number was a number not used by the Radiology Department, i.e. 54321. Once the "patient" file was set up the film could be scanned.

The images were sent to the PACS archive as Dicom files. They were able to be retrieved as TIFF files so they were able to be analysed with the imagej software.

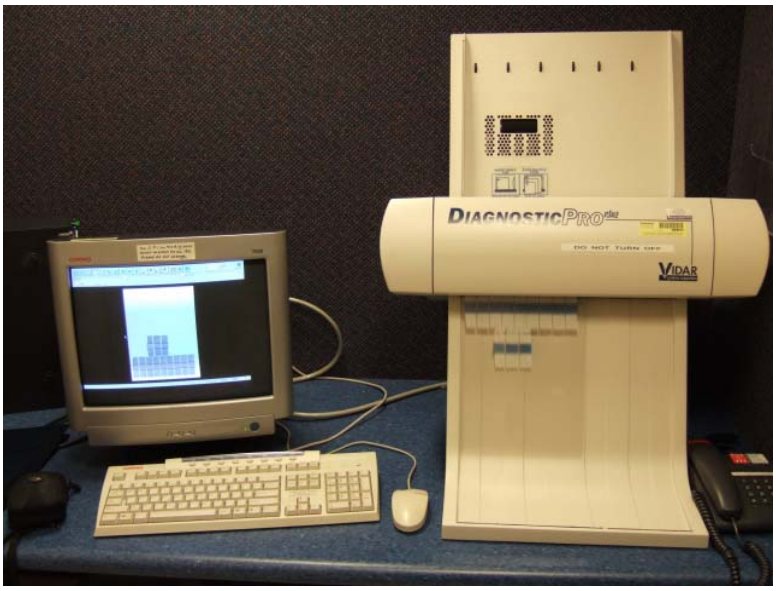

Fig 4.12. Diagnostic Radiology Vidar Scanner.

5. DOSIMETRY THEORY.

5.1 D_{max}

D_{max} represents the depth at which maximum dose occurs within an absorbing medium.

5.2 SSD

The source to surface distance is the distance from the source to the surface of the phantom or patient, where the source is defined as the distance from a point of the surface of the phantom to the focal point of the electron beam. The electron beam is focused on the surface of the target which produces the high energy x-rays.

5.3 SAD

Source to axis distance is the distance from the intersection of the collimator axis of rotation and gantry axis of rotation to the focal point. This is manufactured to be 100cm and is the position of the ionisation chamber for reference condition measurements[15].

5.4 SCD

Source to chamber distance is the distance from to the ionisation chamber being used. This is used if the chamber is positioned at a distance other than the SAD.

5.5 ISL AND ISF

Inverse Square Law is the law which states that radiation radiating from a point will decrease in intensity by a factor of $1/r^2$.

The inverse square factor (ISF) is the factor which is applied to a given intensity (dose) in order to find the intensity (dose) at a greater or smaller distance from the source (Point 2, Fig 5.1), i.e. If a dose is measured at 100cm SAD, using the ISL the

dose at 120cm from the source can be determined. The ISF is the ratio of $1/r_2^2$ and $1/r_1^2$ which yields r_2^2/r_1^2. Therefore $120^2/100^2 = 1.44$. The dose at 120cm is the dose at 100cm SAD divided by 1.44.

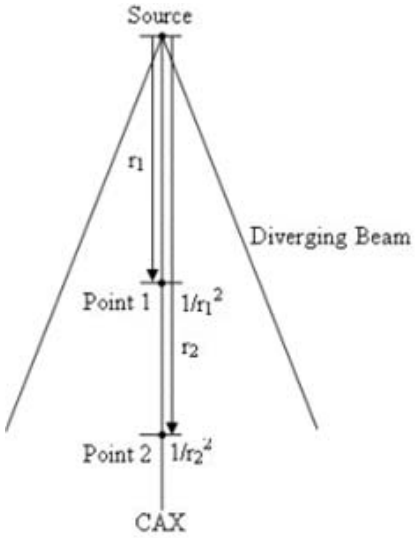

Fig 5.1. This diagram illustrates the difference in distance between two points from the source and the inverse square relationship of each point.

5.6 PDD

A PDD is the quotient, expressed as a percentage, of the absorbed dose at point X by the absorbed dose at point Y. Point X is at any depth *d*, below the surface and the reference point Y is located at a specific depth d_0, below the surface, both being on the central ray[3]. Y is commonly located at d_m, the depth of peak dose. Refer to Fig 5.2.

5.7 TMR

A TMR is the ratio of dose at point X to the dose at point X". X" is at a standard or reference depth d_m, in a phantom but all other conditions of irradiation are the same[5]. Refer to Fig 5.2.

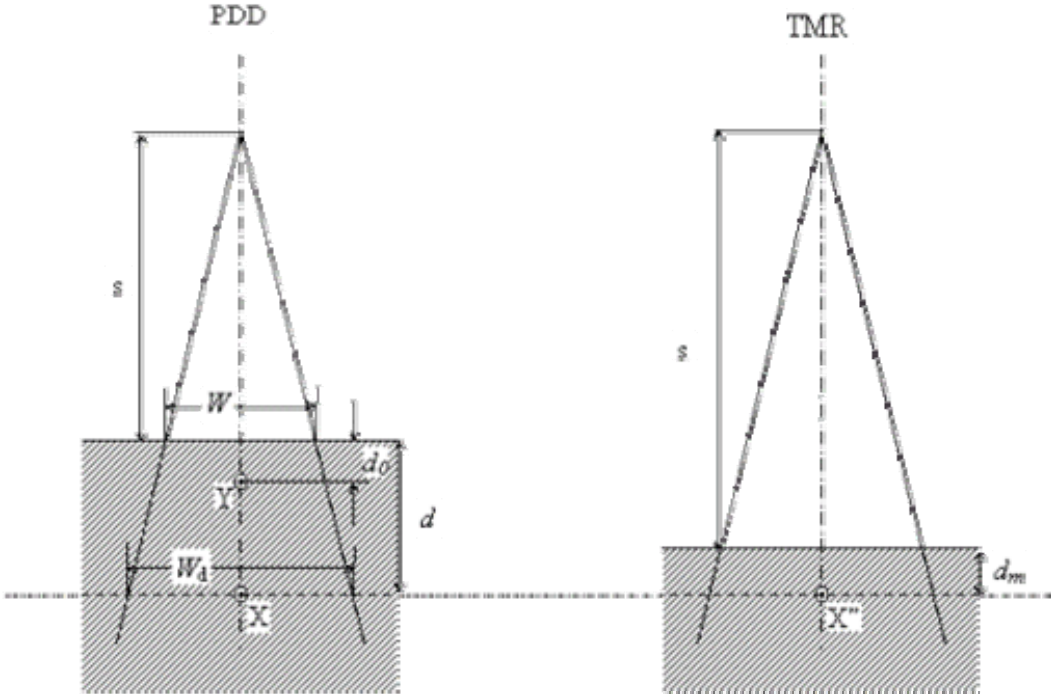

Fig 5.2. These diagrams illustrate the differences between PDDs and TMRs. Adapted from the ICRU Report 24.

5.8 PDD TO TMR CONVERSION.

Converting between PDDs and TMRs can be done either by producing a complete table of PDDs for a large range of field sizes and using the PDD data from the table to determine TMRs for a specific field size, or calculate the TMR using various correction factors. The calculation method is described below.

PDD data are a function of depth, field size, phantom scatter factors (PSF) and the inverse square law (ISL), whereas TMR data are only functions of depth and field size. Converting from PDD to TMR requires the factors correcting for the PSF and ISL. Below is an equation obtained from BJR 25[16] which converts from a PDD to a TMR. The ISL is represented by the function $(f+d/f+d_{max})^2$.

$$TMR(d,S) = \frac{1}{100} \times PDD\left[d, f, S\left(f+d_m\right)/\left(f+d\right)\right] \frac{PSF\left[S\left(f+d_m\right)/\left(f+d\right)\right]}{PSF\left[S\right]} \left(\frac{f+d}{f+d_m}\right)^2$$

Where d is the depth of measurement, S is the field size at d_{max}, f is the source to surface distance (SSD) and PSF is the phantom scatter factor.

Using PDDs the field size at each depth increases due to the divergence of the radiation beam, where each depth is an increasing distance from the source. Using TMRs the field size depth distance remains the same with increasing depth. To convert from a PDD to a TMR each PDD at each depth must be corrected back to a single field size and distance determined at the dmax depth. These corrections are made by the PSFs and ISL previously mentioned. A PSF is a factor which accounts for the increase in scattering material in the beam due to the increase in field size.
The differences between PDDs and TMRs are shown in Fig 5.2.

5.9 SCANNING PDD AND TMR

A scanning PDD and TMR is a PDD or TMR where the field scans across the measurement point instead of remaining stationary.

5.10 MONITOR UNITS (MU).

The monitor unit or MU is the measure of the primary ionisation chamber within the Linac. The sensitivity of the chamber electrometer circuitry is adjusted so that 1 MU is equivalent to a dose of 1cGy[17], where the dose is delivered at d_{max} on the central axis (CAX) of the beam, with a 10 x 10cm^2 field size, at an SSD of 100cm. This sensitivity, 1cGy/MU is measured regularly in quality assurance checks with the conditions described.

5.11 EQUIVALENT SQUARE (ES).

The area of a non-square or irregular field can be represented by an equivalent square field size, simplifying the presentation of dosimetry data (PDD, TMR, etc). Equivalent square fields can be calculated using the equations[17] shown below.

$$a_{eq} = \frac{2ab}{a+b} \quad .$$

$$r_{eq} = \frac{a_{eq}}{\sqrt{\pi}} \quad .$$

Where a_{eq} represents the side of the equivalent square, a and b represent the rectangular field sides, and r_{eq} represents the radius of an equivalent circle.

6.1 METHOD AND MATERIALS.

6.1.1 Scanning Bed.

Rails were placed on the floor of the treatment room approximately perpendicular to the gantry. The separate end of the rails and the attached stepper motor was secured to the main rail section. The stepper motor was connected to a power supply in the treatment room and a controller board which was in turn connected to the controller computer via a cable. The controller computer was situated in the treatment machine console area outside the treatment room. Small metal sheets were used to support the ends of the rails to maintain the level of the rails. The scanning bed was wheeled onto the rails using ramps detailed in the equipment chapter. The scanning bed was then moved up and down the rails ensuring an unhindered movement and to check the alignment with the room lasers. Adjustments were made by moving the rails in the appropriate direction. The phantom was then placed on the bed top and the SSD measured. The scanning bed speed consistency was checked by programming the bed to move 1m and timing the movement. Bed speeds have been tabulated in Table 4.1 in the equipment chapter. The bed speed used for all measurements was 0.706m/min and the consistency check verified this speed. The bed speed allowed for the calculation of the time and MU (monitor units) parameters required for the scan. The time and MU parameters were entered into the console computer.

6.1.2 Phantom Setup for Scanning PDD Measurements.

A large rectangular phantom was used for the scanning PDD measurements. The phantom was constructed using Solid Water blocks and two Perspex cubes filled with water. Phantom dimensions were 90cm x 30cm x 30cm (L x W x H). The Solid Water was placed between the Perspex cubes as in Fig 6.1. The distance to the surface of the phantom was 108.4cm.

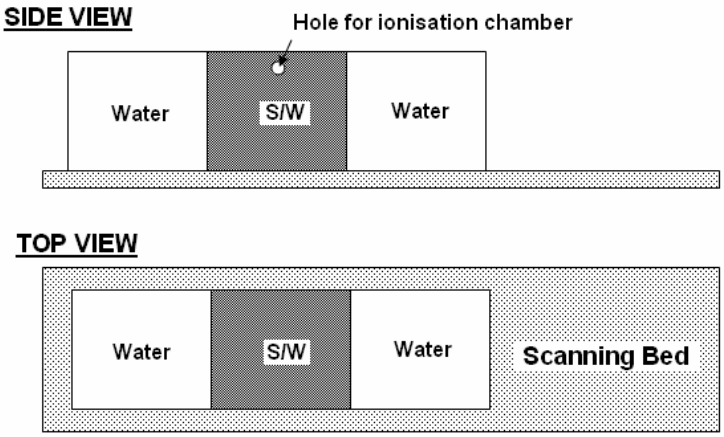

Fig 6.1. Setup of the rectangular phantom on the scanning bed. Also showing the hole for the ionisation chamber.

6.1.3 Phantom Setup for Scanning TMR Measurements and Slit Width Determination.

A large rectangular phantom with 90 x 30cm (L x W) was used. An ionisation chamber was placed at a reference depth of 1.5cm. 8cm of Solid Water was used beneath the chamber. Perspex cubes were used for the 20cm deep measurements as not enough Solid Water was available. Solid Water was placed above the chamber to place the chamber at depths of 5cm, 10cm, 15cm and 20cm. The setup for acquiring TMRs is shown in Fig 6.2.

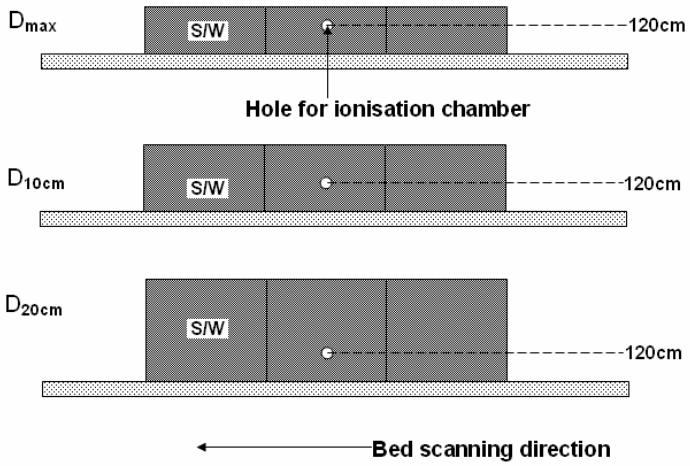

Fig 6.2. TMR setup. Showing when the Solid Water is replaced by Perspex water cubes. Three measurement depths are shown to illustrate the addition of the Solid Water above the ionisation chamber.

6.1.4 Equipment Specifications.

A Farmer 2571 ionisation chamber was used for the measurements and was inserted into a hole in a Solid Water block. The Farmer 2571 chamber was connected to a Farmer electrometer. Temperature and pressure corrections were entered into electrometer. The gantry position was set to 0˚, and the collimator angle set to 90˚. A 6MV photon beam was used for the measurements. Measurements were taken at scanning field sizes of 40 x 10cm^2, 40 x 20cm^2, 40 x 30cm^2, and 40 x 40cm^2 (field sizes refer to the jaw setting). For each scanning field measurements were taken at the following depths: d_{max}, d_5, d_{10}, d_{15}, and d_{20}. At each depth three readings were taken. Fig 6.3 shows the orientation of the jaws relative to the scanning bed. The jaw settings were in the form of X x Ycm^2.

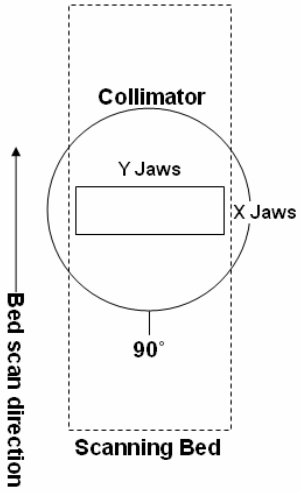

Fig 6.3. Orientation of the collimator jaws relative to the scanning bed, where the jaw settings were of the form X x Ycm^2. The Y jaw settings represent the slit width.

For the scanning PDD measurements, the 40 x 40cm^2 scanning field had measurements taken at the following depths: d_{max}, d_5, d_{10}, d_{15}, and d_{20}. Fields 40 x 10cm^2, 40 x 20cm^2 and 40 x 30cm^2 had measurements taken at the following depths: d_{max}, d_{15}, and d_{20}. The scanning fields started the scans with the leading edge of the light field aligned to the front edge of the phantom. The bed translated until the following light field edge was aligned with the back edge of the phantom as in Fig 6.4.

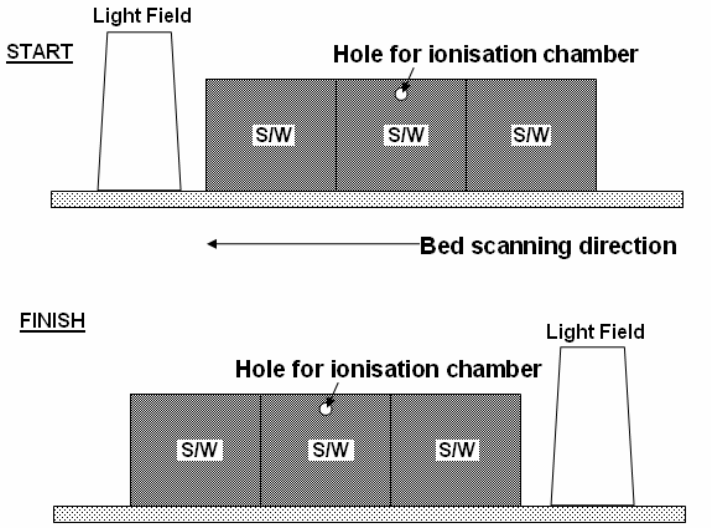

Fig 6.4. Scan setup showing the position of the radiation field at the start and end of the scan and the bed scanning direction.

For the scanning TMR measurements, measurements were taken at scanning field sizes of 40 x 10cm^2, 40 x 20cm^2, 40 x 30cm^2, and 40 x 40cm^2 (field sizes refer to the jaw setting). Refer to Fig 6.2 for the jaw setting orientation. For each field size measurements were taken at the following depths: d_{ref} (1.5cm), d_5, d_{10}, d_{15}, and d_{20}. At each depth three readings were taken. The chamber was positioned 120cm from the source (source to chamber distance, SCD). The bed scan and irradiation were started simultaneously.

6.1.5 Gafchromic EBT Film.

A sample of Gafchromic EBT film[18] was sent from AlphaTech in Auckland. Once the film arrived it was inspected for damage and none was found.
The Film was lot #: 35146 – 005 and was kept refrigerated to extend life.

2 x 2cm^2 squares were cut from the sheets of film. Sharp scissors were preferable over a scalpel or razorblade (scalpel/razor blade caused separation of the film layers). The film layers are shown below in Fig 6.5.

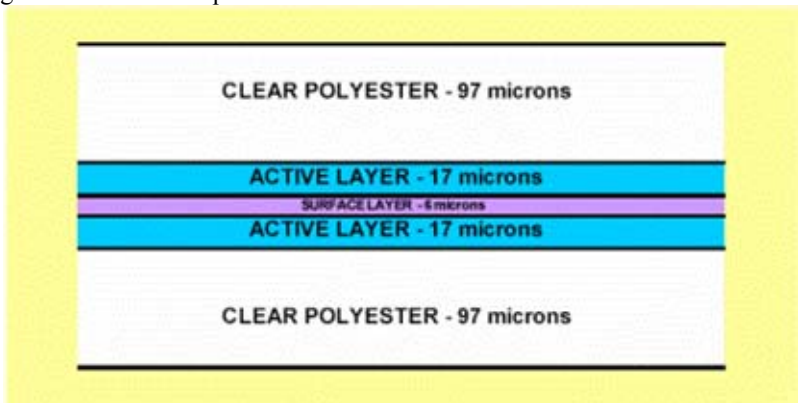

Fig 6.5. Components of the Gafchromic film (ISP Gafchromic-EBT Product Brochure).

This type of Gafchromic film had a different sensitivity depending on the orientation of the film and was caused by the direction of coating the active layers. The coating contains long polymer fibers which when applied to the active layers align in a single direction. In Fig. 6.6 below the direction of the horizontal lines indicates the orientation of the polymer fibers and the coating direction.

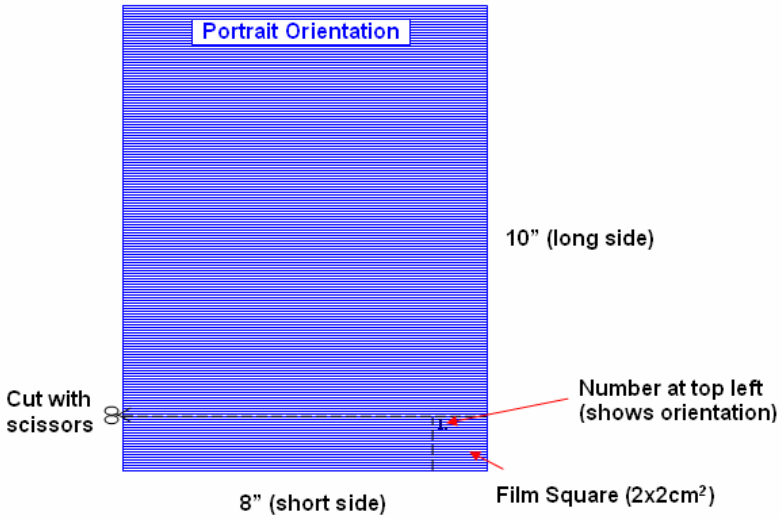

Fig 6.6. Film orientation. Each film square was numbered at the top right of the film to keep film orientation consistent. The coating direction was from the left to the right and aligned the polymer fibers in the horizontal direction.

6.1.6 Film Calibration Setup.

10 film squares were cut and each film square was placed at d_{max} depth (1.5cm) in Solid Water, at 100cm SAD, with 5cm of backscatter Solid Water. The film square was placed at the center of a 10 x 10cm^2 field. This region of the beam was the most uniform and is shown in the beam profiles below (Fig 6.7). The beam energy was 6MV. Fig 6.8 is a schematic of the setup for the film calibration.

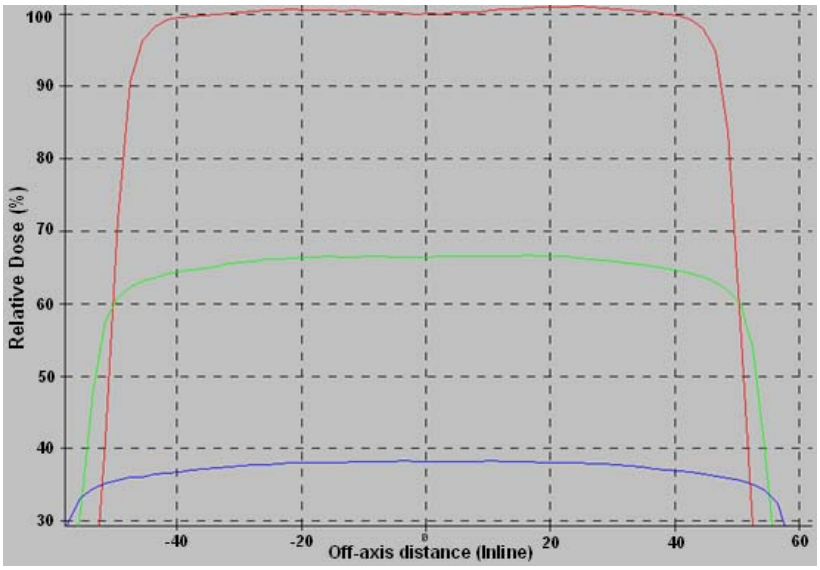

Fig 6.7. Profile measurements of a 10 x 10cm^2 field at several depths. 1cm either side of the central axis has the least variation in relative dose.

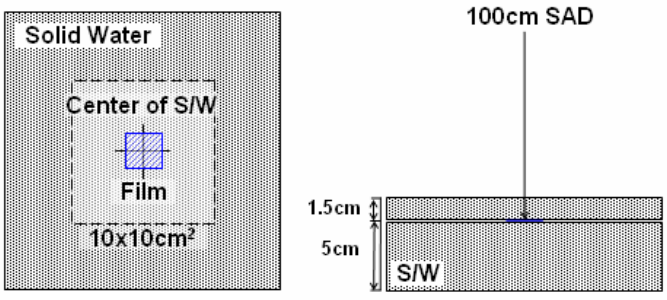

Fig 6.8. Setup used for calibrating film.

Each film square was irradiated with the number of MUs shown in Table 6.1.

#	MUs	1	2	3
1	50	√	√	√
2	75	√	√	√
3	100	√	√	√
4	150	√	√	√
5	200	√	√	√
6	250	√	√	√
7	300	√	√	√
8	350	√	√	√
9	400	√	√	√
10	800	√	√	√

Table 6.1. Initial set of film calibration measurements over the range 50MU to 800MU.

Exposed film squares were left for a period of time to reach maximum density growth. The density growth was taken from the ISP Gafchromic-EBT product brochure[18] and is shown in Fig 6.9 below

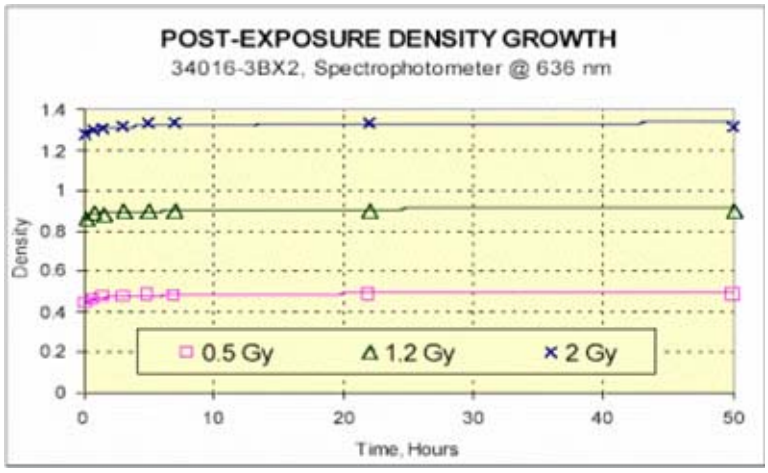

Fig 6.9. Density growth of Gafchromic EBT film. Shows the time period of the density growth (ISP Gafchromic-EBT Product Brochure).

6.1.7 Red Laser Scanner.

The Red Laser scanner was a single 633nm diode laser attached to an aluminium arm. The laser was aligned with a detector also attached to the arm. Between the laser and detector was a plane of glass, where the irradiated film was taped (Fig 6.10). The arm can be programmed to scan in any 2D direction. via the interface with a desktop computer. The software is RFA300 (water tank scanning

software). In the RFA300 software a point to point scan was programmed and used for scanning across the 10 film squares.

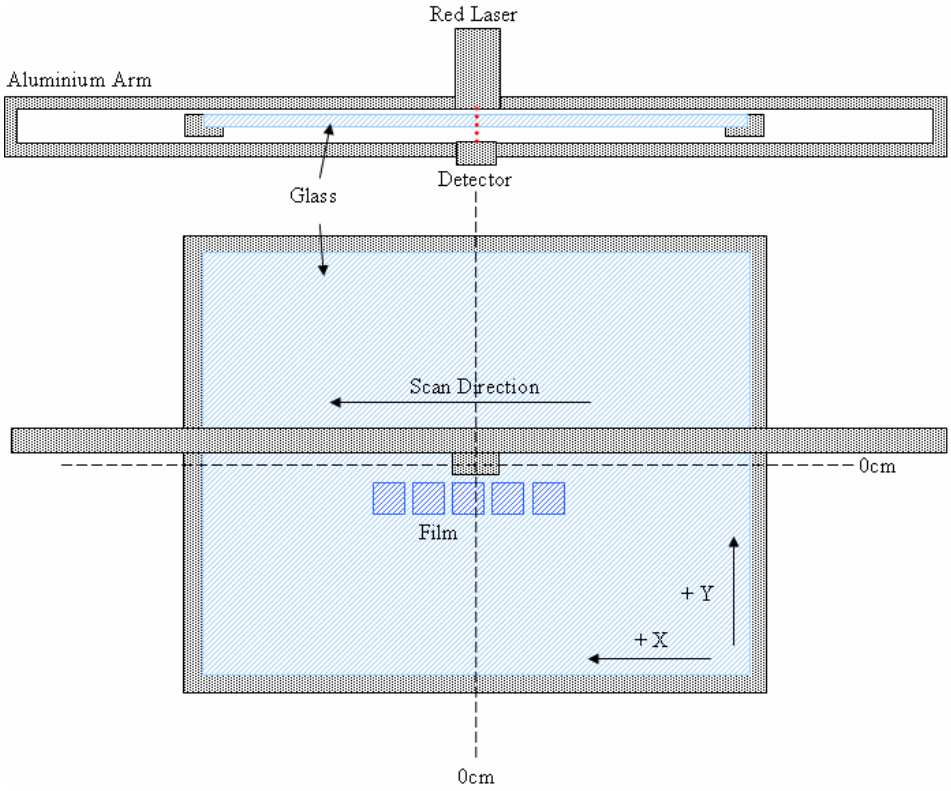

Fig 6.10. Schematic of the Red Laser scanner. Scan direction also shown.

Dark current was taken at a point outside of the film squares. The film readings were normalized to the film with 800MUs. DAT files were created and converted to ASCII files. Excel was used to access the ASCII files for data analysis. The results were poor and an alternative method of acquiring results from the film was found. An X-Rite Visual-light Point Densitometer was used.

6.1.8 X-Rite Visual-light Point Densitometer.

The X-Rite Visual-light point densitometer takes a point measurement using visual (polychromatic) light. A measurement was taken from the center of the film. The densitometer was zeroed after each measurement by taking a measurement with no film present. The readings were recorded and entered into a spreadsheet for analysis. The reading variation was measured. A sample of the 3 film used in the

above measurements was taken and measurements were made at 5 different locations on the individual film squares (Fig 6.11). Each reading was limited to 3 significant places by the readout display.

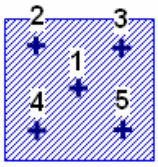

Fig 6.11. Measurements locations for the determining the measurement variation of the X-Rite Densitometer.

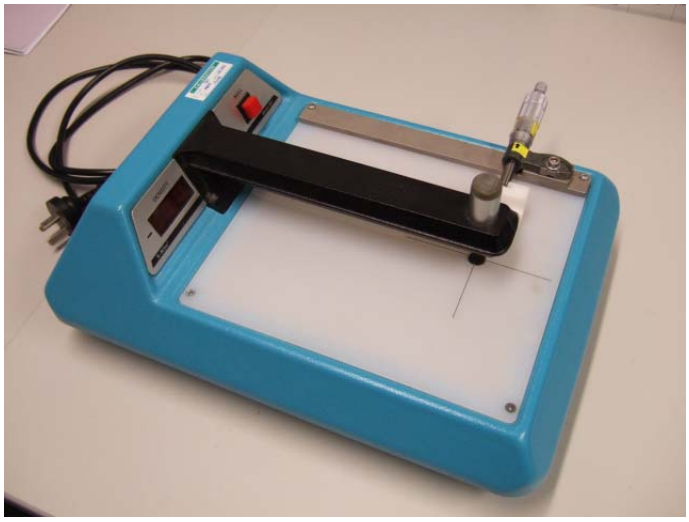

Fig 6.12. Photo of the X-Rite densitometer showing the point measurement device and the readout display with 3 significant figures available.

6.1.9 VXR-16 Vidar Scanner.

The use of a Vidar scanner was investigated. The department Vidar scanner was a VXR-16 scanner. The optical density mode of the scanner was chosen. Pixels in this mode represented the optical density of the film. Analysis of the film images acquired from the vidar scanner required imaging software. The Imagej software (version 1.37) was downloaded from the internet (website http:/rsb.info.nih.gov/ij/) and used for the analysis of the film images. The 3 sets of calibration film used with the red-laser scanner and the X-Rite visual-light point densitometer were scanned in

the VXR-16 Vidar scanner. Each film square was orientated in the portrait direction. The film images were analysed and compared to the X-Rite visual-light point densitometer results. The method of film analysis is shown from Fig 6.13 to Fig 6.15. The prescribed dose to midline was to be 100cGy. A dose range of 50-150cGy was estimated as the range of dose to the midline due to the varying slit widths. A calibration curve in this estimated range was measured. A set of 12 film squares were cut from the Gafchromic-EBT film. Each film square was irradiated with a certain number of MUs (Table 6.2).

#	MU s	Set 1	Set 2	Set 3
0	0	√	√	√
1	50	√	√	√
2	60	√	√	√
3	70	√	√	√
4	80	√	√	√
5	90	√	√	√
6	100	√	√	√
7	110	√	√	√
8	120	√	√	√
9	130	√	√	√
10	140	√	√	√
11	150	√	√	√

Table 6.2. Three sets of calibrated film were irradiated from 50MUs to 150MUs.

The film squares were attached to an OHP sheet and scanned with vidar scanner.

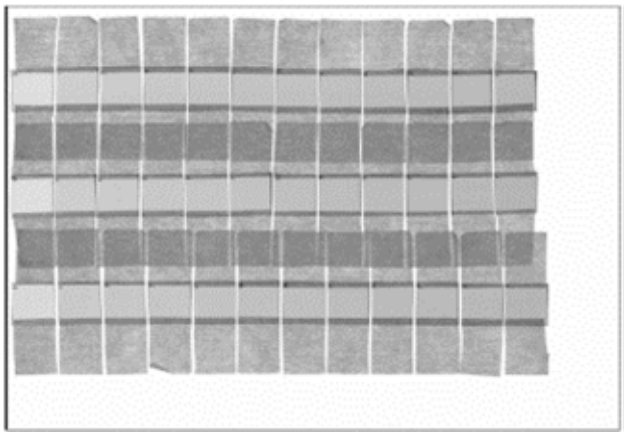

Fig 6.13. Image of film squares attached to an OHP sheet. Each row of film is one film calibration set.

Using imagej a background measurement was done using the box tool option in imagej to drag a box across an area of space where there were no film squares present.

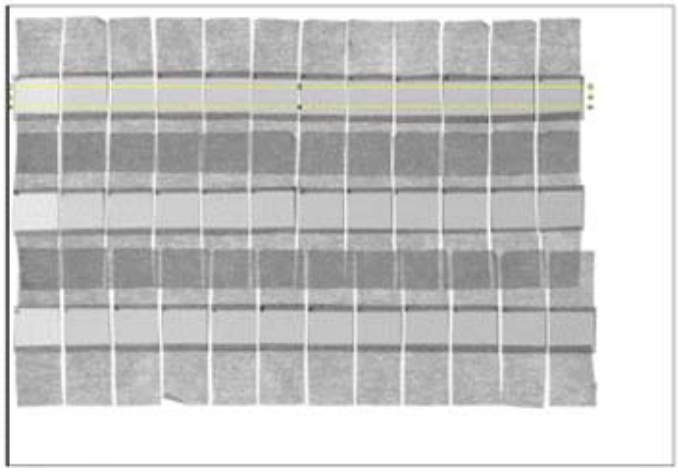

Fig 6.14. The yellow box is dragged across an area that is to be profiled. Here film calibration Set 1 is going to be profiled

Plot profile was then selected from the analyze option in the menu bar. The calibration measurements were done as shown in Fig 6.15. The resulting profile is shown in Fig 6.16. Each horizontal bar represents a film square where the vertical lines are the gaps and edges of the film squares. Optical density increases from left to right.

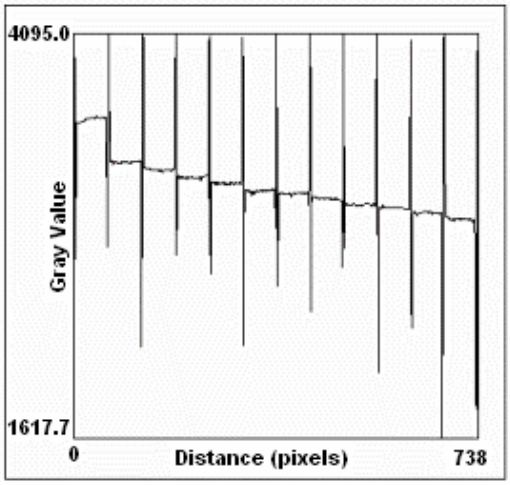

Fig 6.15. Profile measurement of film calibration Set 1.

The data values associated with the profiles (background and film squares) were copied into an Excel worksheet. Here the background data could be removed from the film square profile.

The Vidar Scanner VXR-16 began giving results which were not consistent with prior scans. Below is a scan and profile of a blank OHP sheet (Fig 6.16a) and 6.16b)).

Fig 6.16a) A blank OHP sheet was scanned and above is the acquired image.

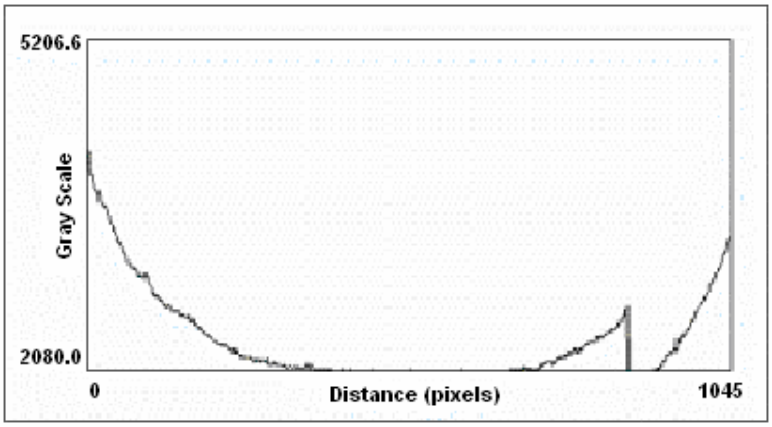

Fig 6.16b). Profile of the blank OHP sheet.

Another Vidar Scanner was available in the Radiology Department. This scanner had been specifically setup for diagnostic radiology work and included the ability to vary the windowing level (a constant window level was chosen). The Mode of scan was linear, and the pixel values were equivalent to the bit size of the image (12-bit image, 4096 grey levels). The type of Vidar Scanner was a Diagnostic Radiology Scanner. The Software installed was Agfa IMPAX TS5. To use this Vidar Scanner a patient file was required to be set up. This involved inputting basic information (First and Last name, NHI (National Health Index) number, current date, M/F). The NHI number used was a number not used by the Radiology Department,

i.e. 54321. Once the patient file was set up a film could be scanned. The images were sent to the PACS archive as Dicom files. They were able to be retrieved from the PACS archive as uncompressed TIFF files and analysed using the imagej software.

6.1.10 Diagnostic Radiology Vidar Scanner Consistency Checks.

The scanner consistency was checked by scanning the film 3 times in the portrait orientation then changing the orientation to landscape. Two scans were done with the film flipped over but remaining in the portrait orientation. Table 6.3 shows the scan orientations.

Scan	Portrait	Flipped	Landscape
1	√		
2	√		
3	√		
4		√	
5		√	
6			√
7			√
8			√

Table 6.3. Orientation of the film as they were scanned.

A measurement was taken at the same point for each image and the resulting pixel values compared.

6.1.11 Dose Uniformity Measurements.

The dose uniformity measurements were done in a rectangular phantom 90cm x 30cm x 20cm (L x W x H) placed on the scanning bed. The depth to the midline was 10cm. The slit width was 19 @ 120cm SMD. Film square placement is shown below in Fig 6.17. The film squares were scanned using the Diagnostic Radiology Vidar scanner. For the scanning bed setup refer to the scanning bed section.

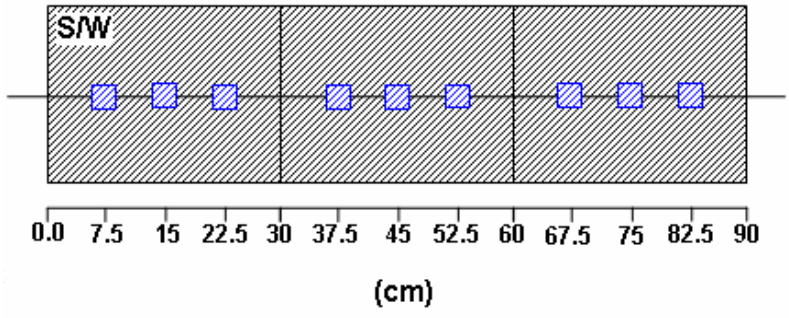

Fig 6.17. Position of the film squares in the rectangular phantom for the dose uniformity test. Beams Eye View (BEV).

6.1.12 Dynamic MLC Dose Step Experiment.

The aim of this experiment was to use a step simulation to determine the precision of the DMLC movement. The step simulation simulates the head/neck region and was the most difficult MLC movement to program. The phantom was separated into 3 segments (Fig 6.18). The first segment would represent the neck and the second segment would represent the chin or head.

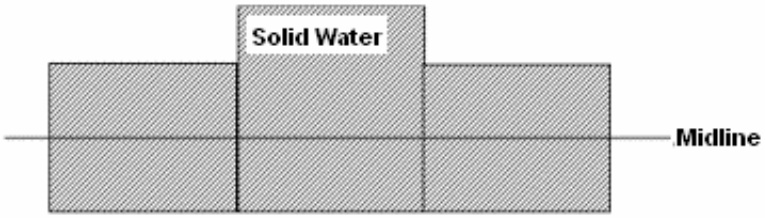

Fig 6.18. Simulated arrangement of the phantom. The simulation was tested using a flat rectangular phantom.

The movements of the DMLC leaves were programmed using the MLC Shaper. Table 6.4 shows the DMLC pattern.

Field	X1	X2	Dose Fraction
1	7.9	7.9	0.0000
2	7.9	7.9	0.4268
3	14.4	7.9	0.4875
4	14.4	7.9	0.5125
5	14.4	1.4	0.5732
6	14.4	1.4	1.0000

Table 6.4. Pattern used to program the DMLC movements. The slit width used was the same slit width used for the dose uniformity test (19cm @ 120cm SMD).

A complex process was required to calculate the dose fractions. Below describes the process for calculating the dose fractions. Figures 6.19 and 6.20 illustrate the movements and distances of the Fields.

1. The first field moves the 5cm to the phantoms' front edge, and continues moving until the fields' following edge has reached the intersection of segments 1 & 2 at the midline. This distance is shown in the Table 6.5.

2. The second field changes to the next required slit width. This change in slit width was done in such a way as to approximate a step increase in dose. As the bed scans in the left direction (Fig 6.19 and Fig 6.20) the fields' following edge moves in the same direction at the same speed. The fields' following edge appears stationary to the bed and phantom.

3. The third field moves along the phantom until the fields' leading edge reaches the intersection of segments 2 & 3 at the midline.

4. The fourth field changes back to the first field slit width. The fields' leading edge' moves in the same direction and speed as the scanning bed.

5. The fifth field moves along the phantom until the fields' following edge has moved 5cm past the phantoms' back edge.

6. The sixth field is the slit width at the end of the scan. There is no further movement.

Fields	Calculation	Distance (cm)
1 to 2	5+30+(20.54-(20.54-19)/2) =	54.77
2 to 3	26.8-19 =	7.80
3 to 4	30-26.8 =	3.20
4 to 5	26.8-19 =	7.80
5 to 6	30+5+19+((20.54-19)/2) =	54.77
Total distance:	54.8 + 7.8 + 3.2 + 7.8 + 54.8 =	128.34

Table 6.5. Dose fraction calculations.

The dose fractions were then calculated by dividing each scan distance by the total scan distance. Below is the dose fraction for the first to second fields (Table 6.4).

$$\text{Dose Fraction} = \frac{54.77}{128.34} = 0.4268$$

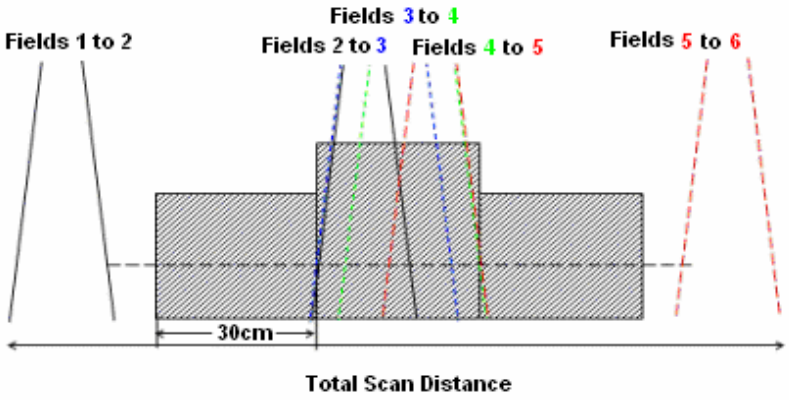

Fig 6.19. DMLC movement across simulated phantom arrangement.

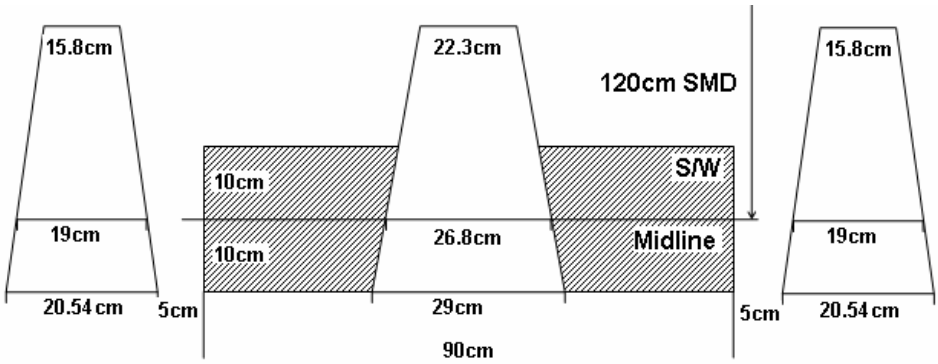

Fig 6.20. Actual phantom arrangement.

2 sets of 10x2cm^2 strips were used. Set 1 film strips were labeled A and B, set 2 film strips were labeled C and D. See Figure 6.21 below.

The second set of film was used as a confirmation of the results. A line was drawn on the 10cm strips showing where the dose step was expected to start and finish.

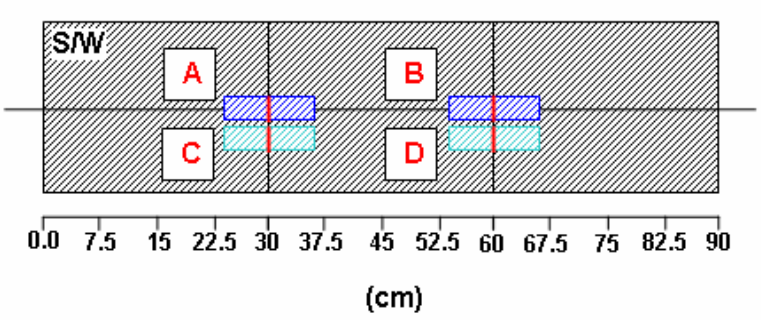

Fig 6.21. BEV of film strip setup on the rectangular phantom.

6.1.13 Comparison of Physical and Simulated Rectangular Phantom Scans.

A rectangular phantom was created in the Xio treatment planning system. The rectangular phantom simulated the phantom used in section 6.1.11. A midline was positioned at 10cm depth and 120cm SMD. The Xio software[19] allowed 99 beams per plan, which limited the beam coverage over the rectangular phantom. The interest points were placed over the first half of the phantom (0 - 45cm) 0.5cm apart to ensure beam penumbra were included in the dose calculations. This resulted in 90 beams being applied. The applied beams had their weight points positioned at each interest point. Each interest point would calculate the dose contribution from each beam. The MUs delivered by each beam were calculated using the equations below,

$$t = \frac{d}{v}$$

$$MU = t \times D/R$$

where d is the beam increment distance, v is the scan speed, t is the time taken for a point to move the beam increment distance, D/R is the machine dose-rate and MU is the number of monitor units delivered for a beam increment. This simulation was then compared to a physical scan. The physical scan used the same phantom setup as the simulation. Placement of the films squares is shown in Fig 6.22. The slit width

used in each experiment was 15.8cm at 100cm SAD, 19cm at 120cm SMD (midline distance).

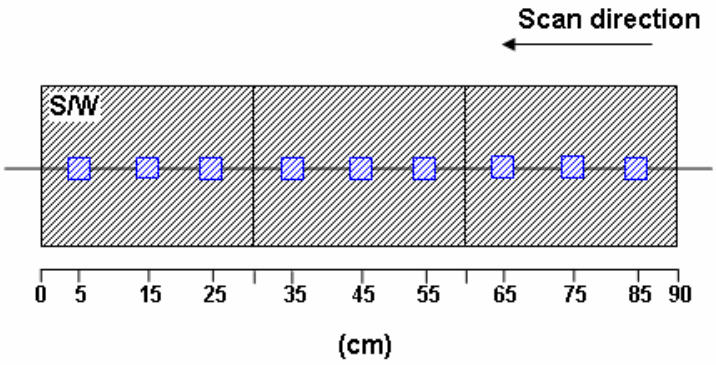

Fig 6.22. Setup of the physical rectangular phantom and the placement of the film squares. Scan direction also shown.

6.1.14 Anthropomorphic Phantom Simulation.

The anthropomorphic phantom was scanned in a GE CT scanner and the images were transferred to a Xio workstation computer. In the Xio planning software the sagittal slices of the CT images were used and the phantom was contoured and the central sagittal slice was chosen. A midline was drawn through the slice and was positioned through the CT scanner iso-center. This position was approximately half-way between the anterior and posterior surfaces of the umbilical region. Interest points were positioned at 1cm intervals along the midline, inferior to superior. Beams were applied with their weight points positioned at each interest point. The beam parameters were: 6MV photons, extended iso-center 100cm SAD plus 20cm (120cm SMD), slit width was to be defined by the physical and/or simulated scan. A total of 92 beams with the same slit width were applied to the phantom. This setup simulated a non-varying or constant slit width (C_{sw}) scanning at a constant speed across the phantom. To simulate a varying slit width (V_{sw}) across the phantom, depth to midline data was required. The depth to midline data for each beam was obtained from the Xio software in the form of a datasheet where the depth to midline for each interest point was available. This data was used for calculating the various slit widths required for a varying slit width scan delivering 100cGy to the midline of the phantom. Dose profiles were taken through a homogeneous phantom. The

homogeneous phantom was created by forcing the electron densities in the CT image to one.

Simulating the V_{sw} was a complex procedure. Referring to Fig 6.23 the starting slit width x scans across the first segment of the phantom with a constant depth to midline. Each point along the midline was exposed to this slit width including the last point on the midline, point P. The slit width must scan into the next segment of the phantom until the following field edge has passed over point P. Each beam was applied taking this extra movement into account. The second segment had an increasing depth to midline which required an increasing slit width to compensate. The rate of change of the slit width can be represented by the relation,

$$v_i = v_b \times \frac{\Delta x}{z}$$

where v_j is the jaw speed, v_b is the bed speed, Δx is the change in slit width and z is the segment distance. Simulating this rate of change the slit width change per beam needs to be determined. This was found by substituting the number of beams along z for z into the equation $\Delta x/z$. Therefore each applied beam slit width from slit width x to $x + \Delta x$ was incremented by $\Delta x/No.\ of\ beams$. The slit widths of each beam were increased using asymmetrical jaws and moving the following jaw by the previously determined increment until the slit width $x + \Delta x$ was reached. The third segment had a decreasing slope where the following jaw moved by pre-determined increments from x_1 to $x_1 - \Delta x_1$. The fourth segment represented the neck and was flat requiring no change in slit width. The fifth segment represented the head. This was the step simulation and the movement was described in the section 6.1.12.

Applying each beam required an understanding of the specific movements detailed above.

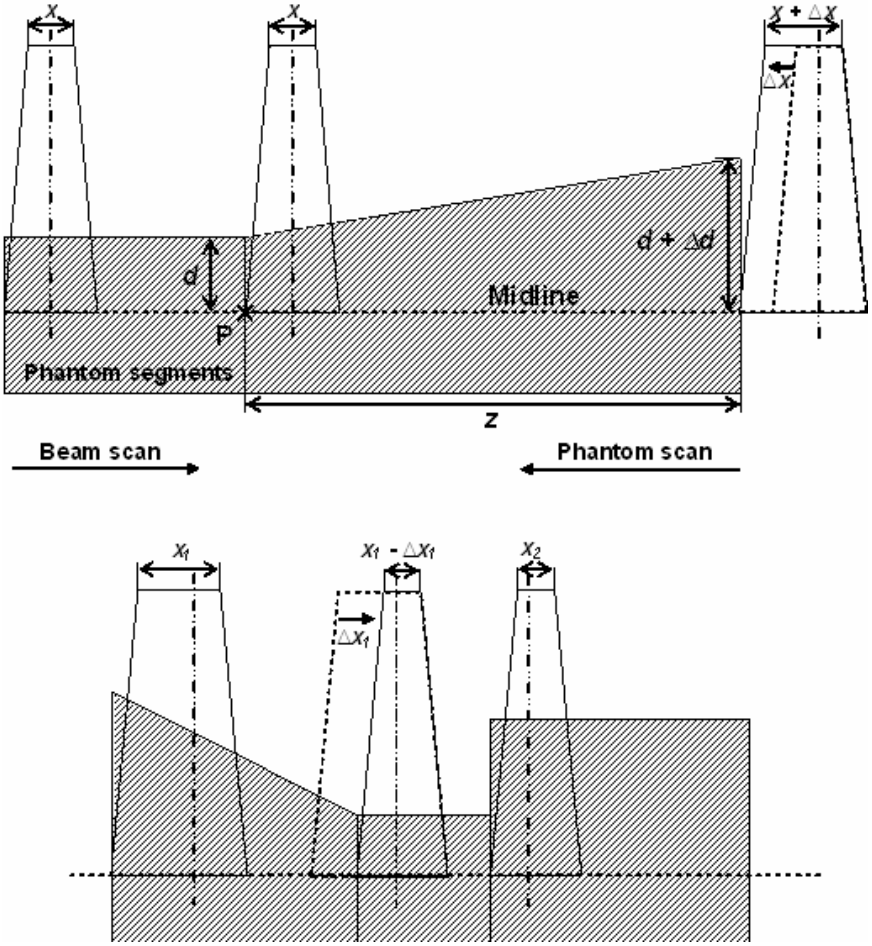

Fig 6.23. Application of beams across the junction of each phantom segment. Each segment is a simplification of a portion of the anthropomorphic phantom.

6.2 RESULTS.

6.2.1 Scanning PDD Measurements.

Corrections were applied to the readings to give absolute doses at each depth for each slit size. The readings were converted into PDDs and the results are shown in the table below.

Slit Size	Depth (cm)	Reading	Slit Width (cm)	In-Beam Time (min)	Reading/min	PDD (S)
40 x 40cm²						(30x43.3cm²)
	1.5	368.5	43.9	0.62	575.9	100.00
	5	324.1	45.3	0.64	504.5	87.60
	10	270.7	47.3	0.67	403.6	70.09
	15	219.3	49.3	0.70	313.8	54.49
	20	178.6	51.3	0.73	245.6	42.65
30 x 40cm²						(30x32.5cm²)
	1.5	266.3	33.0	0.47	568.2	100.00
	15	164.6	37.0	0.52	313.9	55.25
	20	133.4	38.5	0.55	244.5	43.03
20 x 40cm²						(30x21.7cm²)
	1.5	173.4	22.0	0.31	557.0	100.00
	15	108.8	24.7	0.35	311.2	55.87
	20	88.1	25.7	0.36	242.2	43.49
10 x 40cm²						(30x10.8cm²)
	1.5	85.1	11.0	0.16	546.8	100.00
	15	53.1	12.3	0.17	304.2	55.63
	20	43.1	12.8	0.18	237.1	43.36

Table 6.6. This is a table showing the scanning PDDs for each slit size. The slit size represents the jaw settings. The slit width column shows the slit widths at each depth of measurement. The in-Beam time is the time the ionisation chamber was in the beam as it scanned across the phantom. The reading/min column shows the readings which have been corrected for the time the ionisation chamber spent in the beam.

6.2.2 Scanning TMR Measurements.

After acquiring the data, the readings were converted to absolute doses using a measured output factor of 1.019cGy/MU. The scanning TMRs were calculated from the average readings.

Slit size (cm^2)	Depth (cm)	Ave. Reading	Measured Dose (cGy)	Scanning TMR
12x30				ES 16cm
12	1.5	73.6	75.0	1.000
	5	69.3	70.6	0.942
	10	60.7	61.9	0.825
	15	52.3	53.3	0.711
	20	44.5	45.3	0.605
24x30				ES 26.4cm
24	1.5	151.8	154.7	1.000
	5	141.8	144.5	0.934
	10	124.6	127.0	0.821
	15	107	109.0	0.705
	20	90.8	92.5	0.598
36x30				ES 32.4cm
36	1.5	232.1	236.5	1.000
	5	216.4	220.5	0.932
	10	189.6	193.2	0.817
	15	162.4	165.5	0.700
	20	137.6	140.2	0.593
48x30				ES 34.5cm
48	1.5	314.5	320.5	1.000
	5	293.6	299.2	0.934
	10	256.2	261.1	0.815
	15	218.5	222.7	0.695
	20	184.9	188.4	0.588

Table 6.7. The slit sizes represent the field size at 120cm SMD. The average reading was converted to dose (cGy) using a measured Output Factor 1.019cGy/MU. Scanning TMRs were calculated from the readings.

Scanning TMRs for each equivalent square (ES) field size were compared. Fig 6.24 and Fig 6.25 illustrate the similarity of the scanning TMR curves. Lines were drawn between the points to indicate the similarity between the curves.

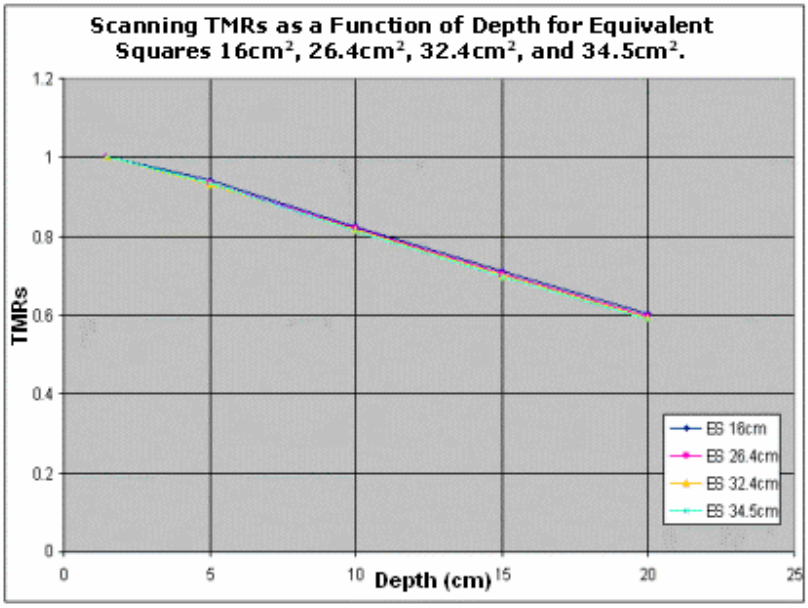

Fig 6.24. Shown here are scanning TMRs as a function of depth for each equivalent square field size. Each Scanning TMR curve varies little from the other scanning TMRs. At depth the scanning TMR curves show the greatest variation.

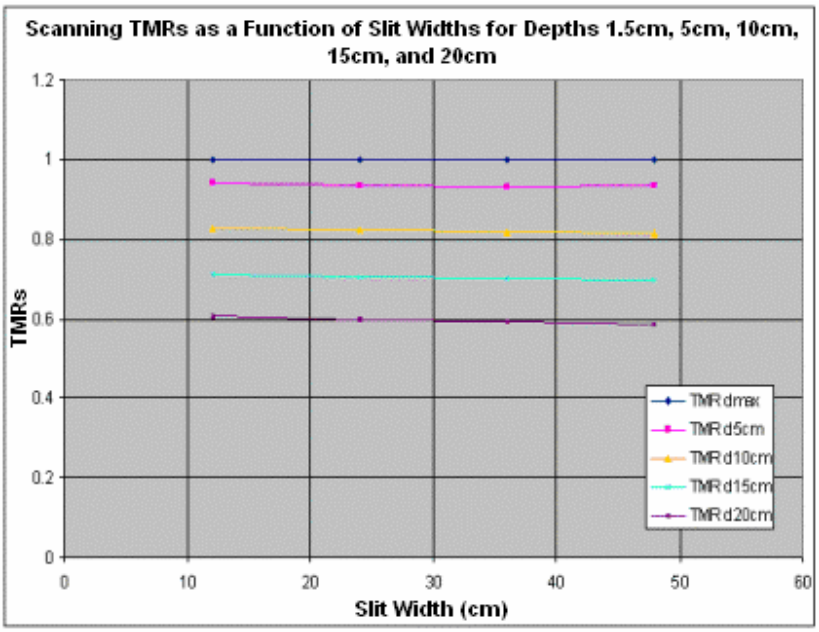

Fig 6.25. This graph shows the variation of the scanning TMR curves as a function of slit width.

6.2.3 Slit Width Measurements.

To ascertain the scanning slit width required to deliver the prescribed dose of 100cGy at the midline depth of 10cm, the dose values were graphed against the slit widths at depths of 1.5cm, 5cm, 10cm, 15cm and 20cm (Fig 6.26).

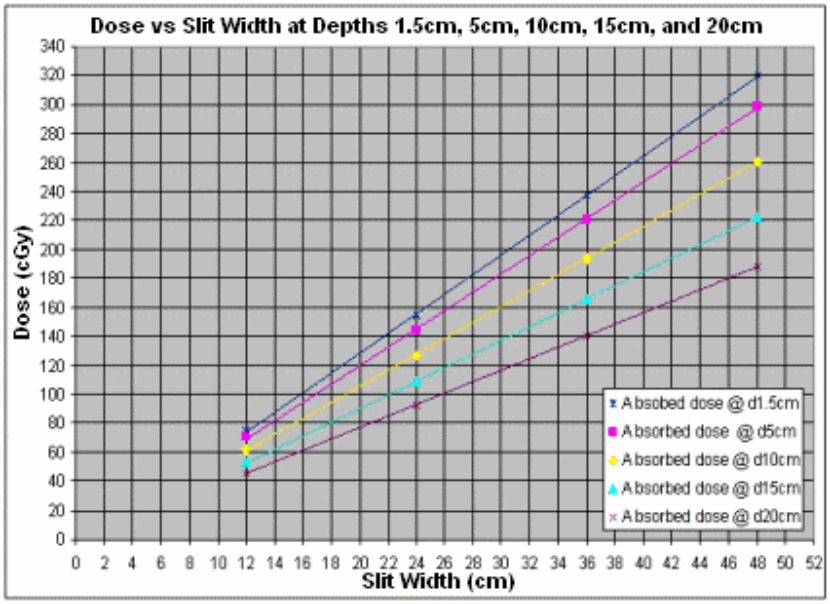

Fig 6.26. This graph displays the absorbed dose measured from within the rectangular phantom against increasing slit width. Normalizing to the reference depth (1.5cm) gives the TMRs shown in Fig 6.24 and Fig 6.25. Increasing the slit width linearly increases the absorbed dose to the phantom.

The dose gradients were caused by the increasing slit widths. A larger slit width causes a point within the phantom to be exposed to the radiation beam for a longer period of time. Therefore a larger slit width will allow the ionisation chamber to absorb a larger dose. Normalizing the doses to the reference depth dose gives the scanning TMRs, as seen in Fig 6.26.

6.2.4 Slit Width Calculations.

Fig 6.27 shows how linearly the dose increases with increasing slit width. Using the linear equation below (Excel.), where y = dose (cGy) and x = slit width (cm), the absorbed dose at 10cm depth can be calculated.

$$y = 5.5323x - 5.1969$$

Rearranging to find the slit width gives,

$$x = \frac{(y + 5.1969)}{5.5323}$$

For a prescribed dose of 100cGy the slit width was calculated to be 19.02cm.
Slit widths were also calculated for the depths 1.5cm, 5cm, 10cm and 20cm (Table 6.8).

Depth (cm)	Slit Width (cm)
1.5	15.82
5	16.81
10	19.02
15	22.00
20	25.82

Table 6.8. Slit widths delivering 100cGy to the depths 1.5cm through to 20cm.

Table 6.8 is graphed in Fig 6.28 and illustrates that with increasing depth the slit width required to deliver 100cGy increases proportional to a polynomial function.

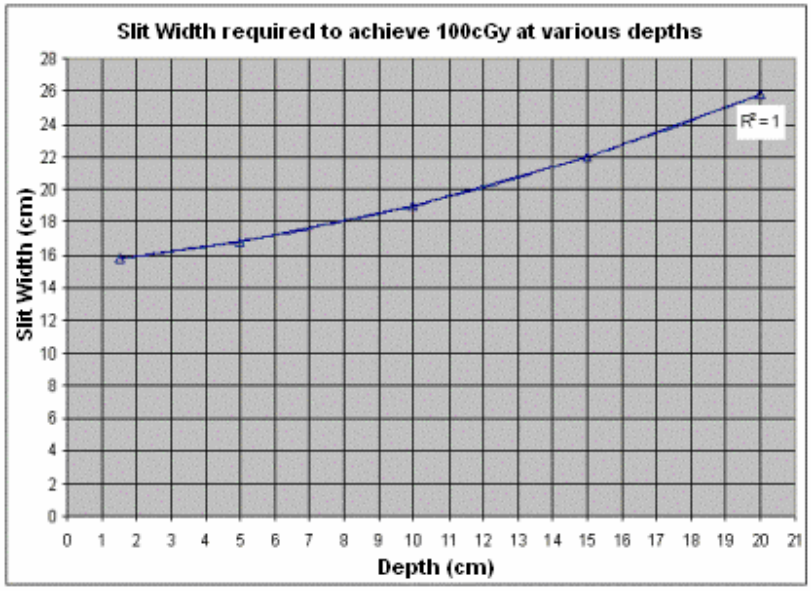

Fig 6.27. With greater depth the slit width required to achieve 100cGy increases proportional to a polynomial function.

A second order polynomial was fitted to the data points and gives the equation below, where 'x' is the depth (cm).

$$y = 0.0169x^2 + 0.1854x + 15.496$$

The fitted polynomial shows an R^2 value of 1 which indicates that the fit is accurate. A comparison of the calculated slit widths from Fig 6.27 and the calculated slits widths from Fig 6.28 was done to confirm the R^2 value. Table 6.9 confirms the relationship.

Depth (cm)	Linear (cm)	Polynomial (cm)
1.5	15.82	15.81
5	16.81	16.84
10	19.02	19.00
15	22.00	21.99
20	25.82	25.80

Table 6.9. Comparison between the polynomial calculated slit widths and linear calculated slit widths.

6.2.5 Red Laser Scanner.

The film squares were scanned using a red laser scanner. Fig 6.28 shows the noise associated with the Red Laser scanner. The points occurring at or near zero are due to the gaps between each film square.

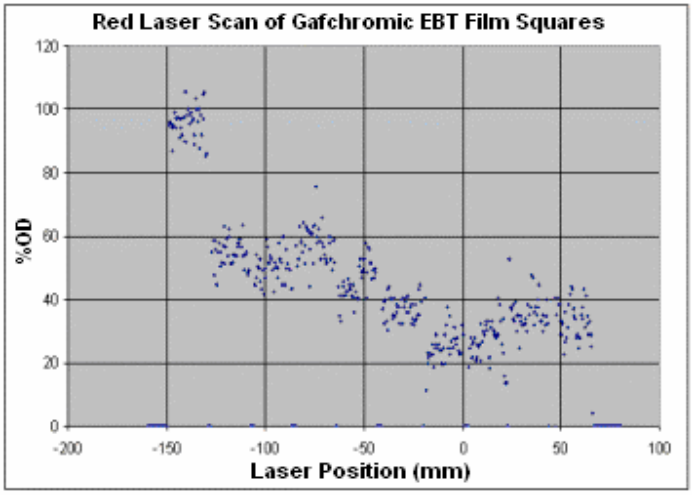

Fig 6.28. Illustrates the amount of noise associated with the red laser scanner. The scanning direction of the laser was from the right to left.

Average readings of each film are indicative of the trend of the optical density readings versus monitor units (Fig 6.29). A second order polynomial was fitted to the data to show the trend clearly.

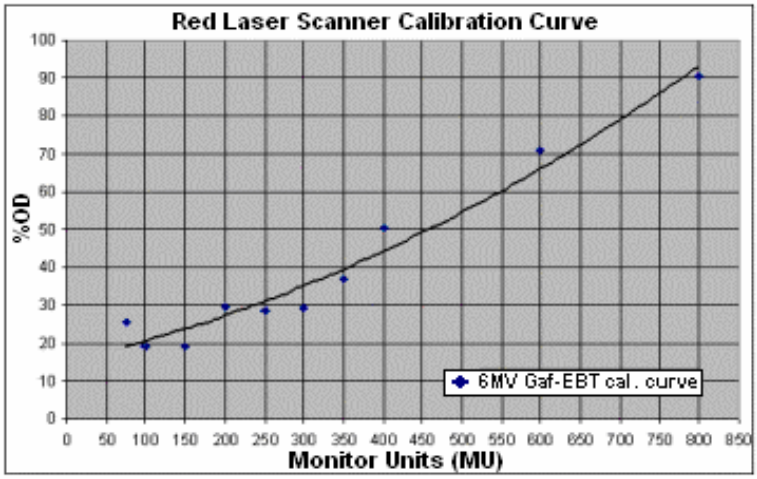

Fig 6.29. Graph showing the results from a scan using the red-laser scanner.

The curve in Fig 6.29 was not consistent with a standard calibration curve. This scanner proved to be unsuitable for calibrating film. A possible cause may have been the absence of the diffusing plate. The results from the Red Laser Scanner were then compared to a visual light point densitometer (X-Rite). The Red Laser scanner was not used for future measurements.

6.2.6 X-Rite Visual-light Point Densitometer.

The X-Rite densitometer showed a consistent increase in density. The range of readings was small, 0.10-0.60, and is shown in Table 6.10. The results are graphed in Fig 6.30. The calibration curve is consistent with the expected form of calibration curves as shown in Fig 6.31 (visual density -black line).

MUs	Dose (cGy)	Ave. Readings	Zeroed Readings
0	0	0.10	0.00
75	75	0.21	0.11
100	100	0.25	0.15
150	151	0.31	0.21
200	201	0.36	0.26
250	251	0.39	0.29
300	301	0.44	0.34
350	351	0.46	0.36
400	401	0.51	0.41
600	602	0.60	0.50
800	803	0.69	0.59

Table 6.10. Corrected dose readings and zeroed Optical Density readings. OD readings found using the X-Rite Densitometer.

Reading variation of the X-Rite was measured and Table 6.11 shows the readings and the associated average reading, range of readings and the percent error. As the readings can only give a reading down to 0.01, this is taken as the reading error.

	Film		
Reading	A	B	C
1	0.24	0.24	0.25
2	0.24	0.25	0.26
3	0.24	0.24	0.25
4	0.25	0.25	0.25
5	0.25	0.24	0.25
AVERAGE	0.244	0.244	0.252
RANGE	0.010	0.010	0.010
%ERROR	4.10%	4.10%	3.97%

Table 6.11. Reading variation from measuring optical density of the Gafchromic film.

Two more sets of calibration film were irradiated and the orientation kept consistent for each film square. Another two sets of results were acquired from the red-laser scanner and the visual-light densitometer. A total of three film calibrations were done (Table 6.10). The red-laser scanner continued to produce the same inconsistent, noisy results.

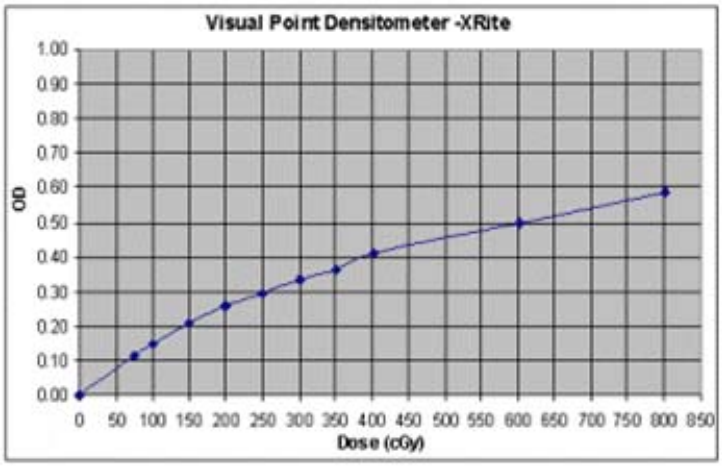

Fig 6.30. Results from the visual point densitometer film calibration.

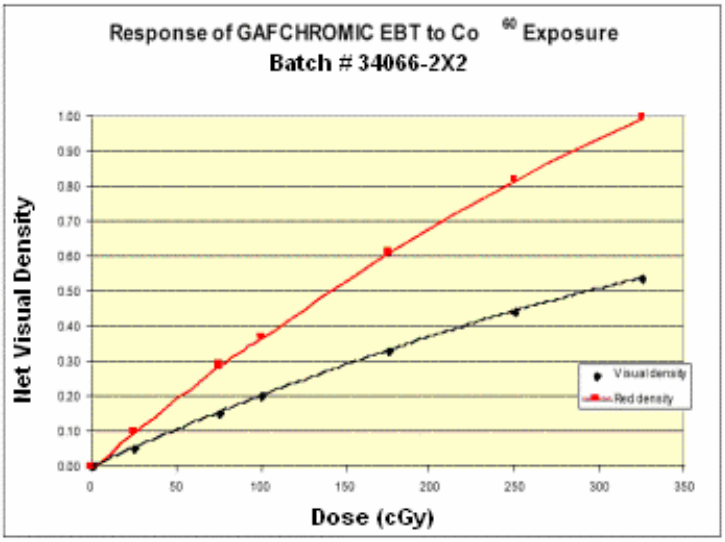

Fig 6.31. Results from developers brochure show expected calibration curves. The red line is Red density and the black line is Visual density. (courtesy of the ISP Gafchromic-EBT Product Brochure).

A comparison was made between the Red Laser scanner results and the X-Rite densitometer results. Fig 6.32 shows the difference between the calibration curves.

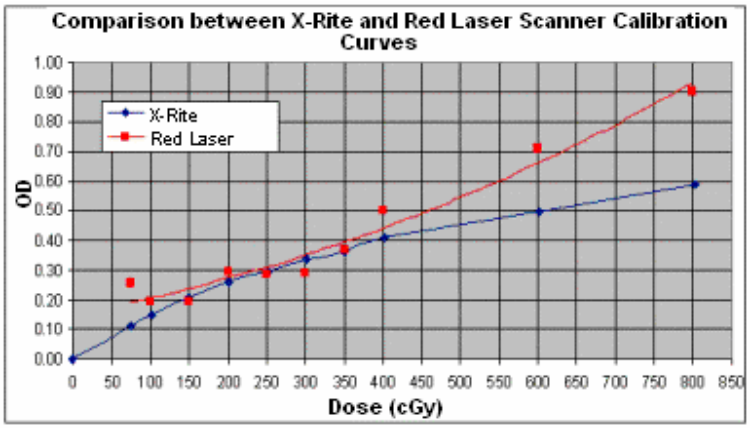

Fig 6.32. The difference between the calibration curves acquired from the Red Laser scanner and the X-Rite densitometer.

6.2.7 VXR-16 Vidar Scanner.

Each set of measurements were converted to percentage optical densities for an equivalent comparison to the X-Rite densitometer. The vidar scanner results compared well with the visual-light point densitometer. An advantage of the vidar scanner was its greater resolution over the visual-light point densitometer making it easier to distinguish between each film square measurement. The X-Rite densitometer supplied readings which were 3 significant figures, this made it difficult to distinguish between each film square measurement.

The sensitivities of vidar scanner and X-Rite densitometer were similar. Fig 6.33 and Fig 6.34 show the individual calibration curves from the VXR-16 scanner and the X-Rite densitometer respectively. At higher doses (above 200cGy) the Vidar scanner had a greater sensitivity. This can be seen in Fig 6.35. The Vidar scanner was subsequently used in place of the X-Rite densitometer.

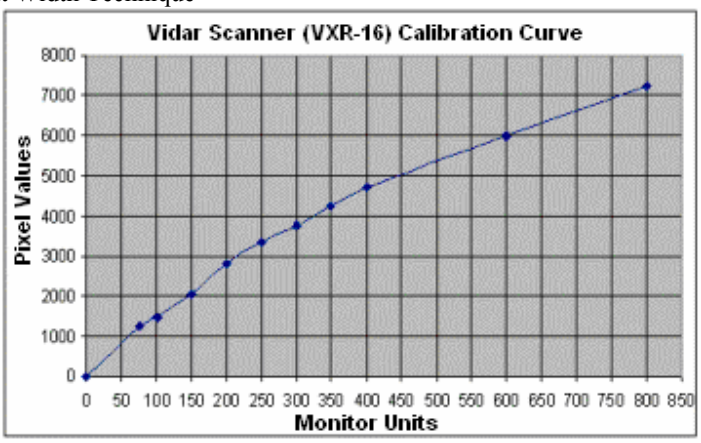

Fig 6.33. Average calibration curve from film scanned using the Vidar Scanner. Monitor Units were compared to pixel value, where the pixel values represented the optical density.

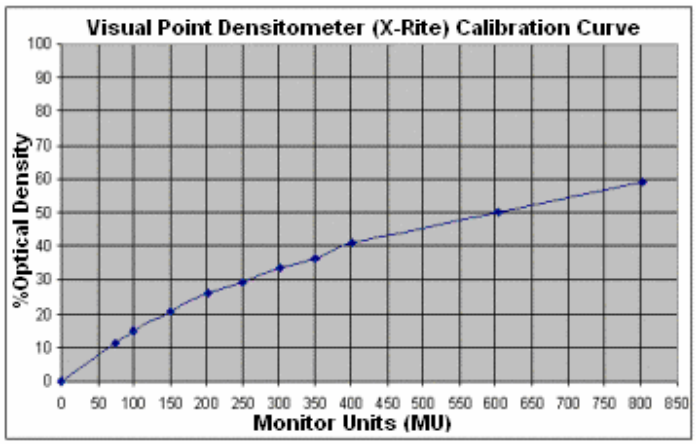

Fig 6.34. Average calibration curve from film using the X-Rite densitometer.

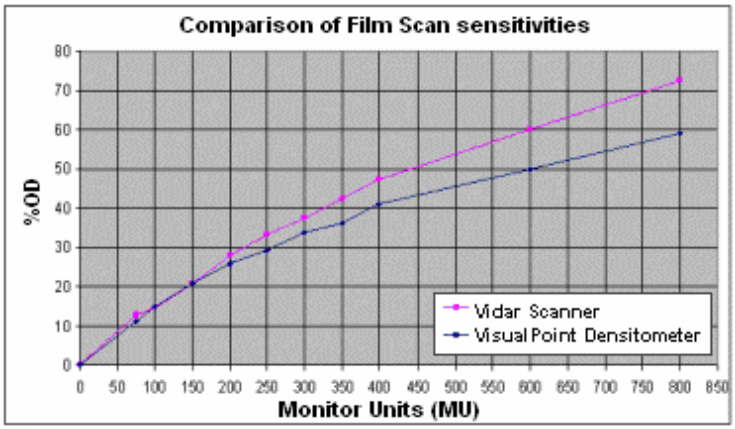

Fig 6.35. Comparison of the Vidar scanner calibration curve and the X-Rite calibration curve. The Vidar scanner has a greater sensitivity above 200cGy than the X-Rite scanner.

The VXR-16 vidar scanner began giving poor results so the diagnostic radiology vidar scanner was used for the rest of the investigation. Measurements were then made over the new dose range of 50-150cGy using the diagnostic radiology vidar scanner. The profile measurements were divided into the corresponding film squares. Background was removed from the film squares, and an average pixel value calculated. 1 standard deviation was used to define the uncertainty of the pixel values. The average pixel values for each film square were then graphed against dose. Set 1 (σ = 8.3), Set 2 (σ = 10.6), and Set 3 (σ = 10.4) are shown below in Fig 6.36. Set 2 does not agree well with Set 1 and Set 3 and was removed. Set 1 and 3 were averaged (σ_{ave} = 9.3) and a linear trendline was fitted to the calibration curve (Fig 6.37).

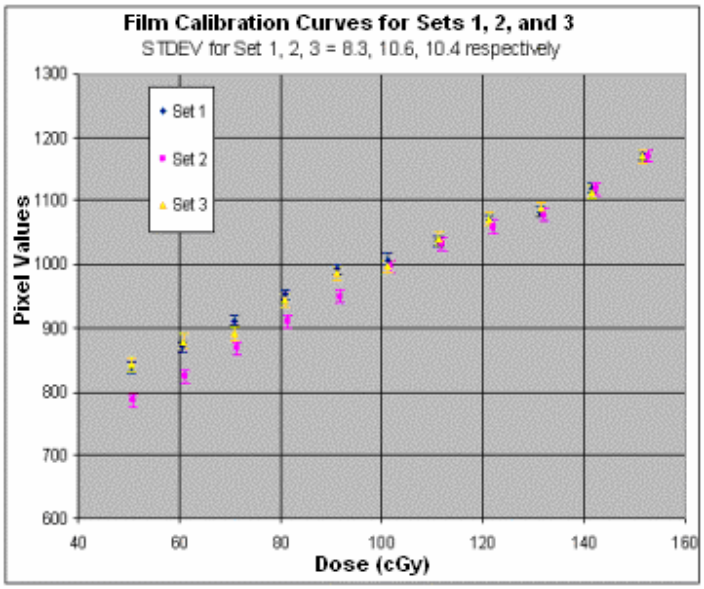

Fig 6.36. This Graph shows the three sets of calibrated film using the Diagnostic Radiology Vidar Scanner. Set 2 diverges from Set 1 & 3.

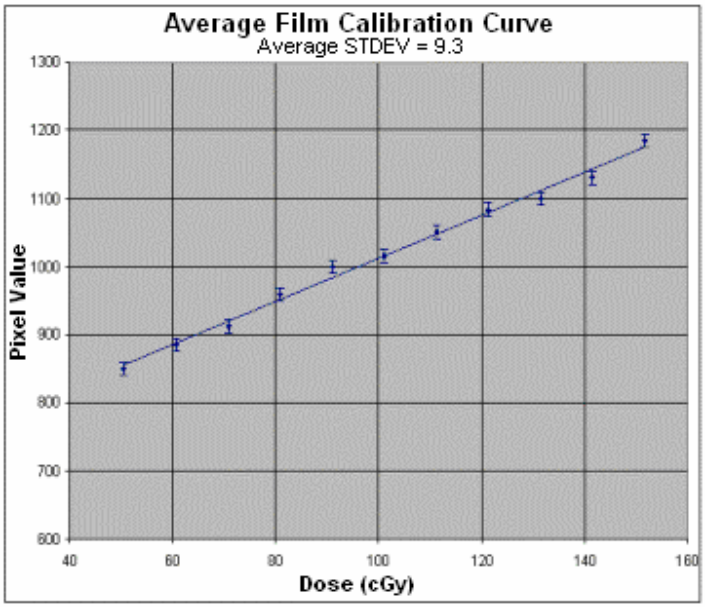

Fig 6.37. Average film calibration curve using Diagnostic Radiology vidar scanner. This region of the curve is close to linear.

These results indicate that a pixel value (after the removal of the background) of approximately 1010 represents a dose of 100cGy.

6.2.8 Diagnostic Radiology Vidar Scanner Consistency Checks.

Table 6.12 shows that the portrait orientations are consistent (including the flipped film). The window levels for the landscape orientation were not consistent with each and different from the window levels for the portrait orientations. This would cause the pixel values of each film scanned in the landscape orientation to be different, as well as being different from the film scanned in the portrait orientation. Future scans were done with the film in the Portrait orientation.

Scan	Ave. Px Value	Window Level
1	3191.5	2519, 1481
2	3191.7	2519, 1481
3	3191	2519, 1481
4	3197.6	2519, 1481
5	3197.3	2519, 1481
6	2981.7	1419, 931
7	2951.8	1391, 917
8	2956.9	1393, 918

Table 6.12. Scans 1 to 3 represent the film in the portrait orientation, 4 and 5 were the flipped film squares and 6 to 8 were the film in the landscape orientation.

These results indicated that the Diagnostic Radiology Vidar Scanner introduced very little error in the film measurements and that the portrait orientation gave the most consistent readings.

6.2.9 Spot Check Measurements.

Three film squares were irradiated with 70, 100 and 130MUs as a spot check for the calibration curve in Fig 6.38. The film squares were scanned in the Diagnostic Radiology scanner.

The pixel values of the three spot check film squares were compared to the calibration curve. A large offset was observed. Fig 6.39 shows the difference in the results.

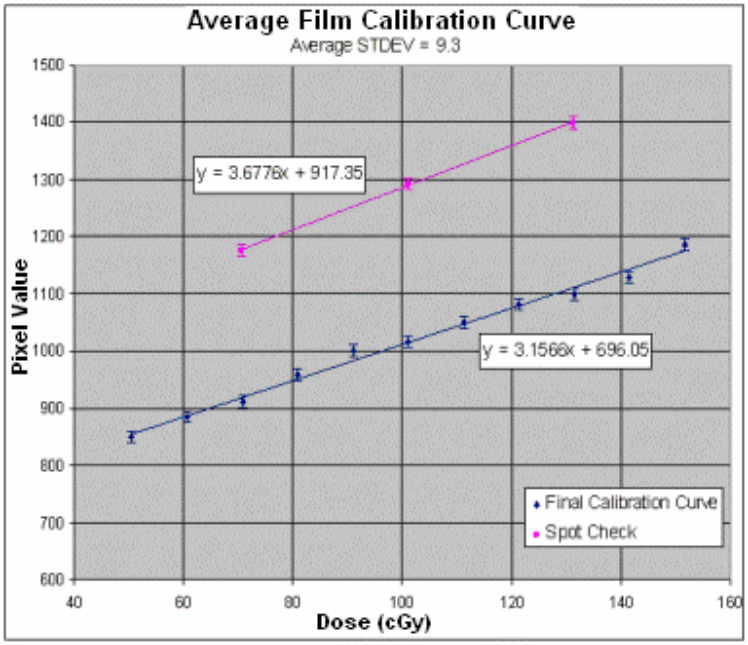

Fig 6.38. Spot check measurements were compared to the calibration curve, a large offset in the results was observed.

Both sets of measurements were done using the same setup. The windowing level was kept constant. No reason could be determined for this large difference in the results. One difference in the procedure was a change of location of the vidar scanner. It was assumed this would not cause such an effect to the pixel value results. Setting

changes within the software were a possible cause as the scanner was freely accessible to everyone.

The spot check film squares were irradiated at the same time as the physical scan of the rectangular phantom described in section 6.2.13. A linear curve was fitted to the spot check points (Fig 6.38) and the equation used to determine the dose to the film squares in the rectangular phantom.

6.2.10 Dose Uniformity Measurement.

The film squares were scanned using the Diagnostic Vidar scanner to give the results shown in Fig 6.39. Using the data acquired from the images the percentage variation across a film square was calculated. The maximum standard deviation from all film squares was 0.91% and can be seen in Table 6.13.

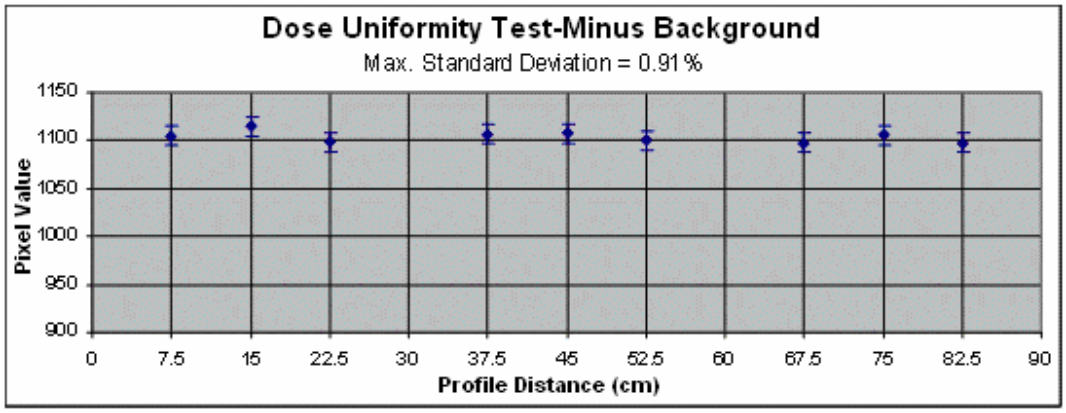

Fig 6.39. Uniformity test using a slit width of 19cm at 120cm SMD. The film was scanned using the Diagnostic Vidar scanner.

The dose uniformity was determined by averaging the pixel value from each film square. The standard deviation was calculated and converted into a percentage. The dose uniformity at 10cm depth, along the midline of a rectangular phantom had a percent variation of 0.53% from the average pixel value.

Film No.	Position	Ave. Pixel Value	%STDEV
1	7.5	1104.733	0.91%
2	15	1114.888	0.39%
3	22.5	1098.375	0.61%
4	37.5	1106.835	0.70%
5	45	1107.969	0.66%
6	52.5	1100.295	0.50%
7	67.5	1097.634	0.81%
8	75	1105.690	0.80%
9	82.5	1097.325	0.46%
AVERAGE:		1103.749	
%STDEV:		0.53%	

Table 6.13. Shown here are the film square positions, the average pixel value of each film square and the associated percent standard deviation. At the bottom of the table the average pixel value of all the film squares and the associated percent standard deviation are shown.

6.2.11 Dynamic MLC Dose Step Experiment.

The figures below show that the DMLC does perform a step increase in dose. The peaks show the where the junction of each phantom segment occur. The difference between the peaks and the 50% of the step gradient determine the offset of the DMLC movement.

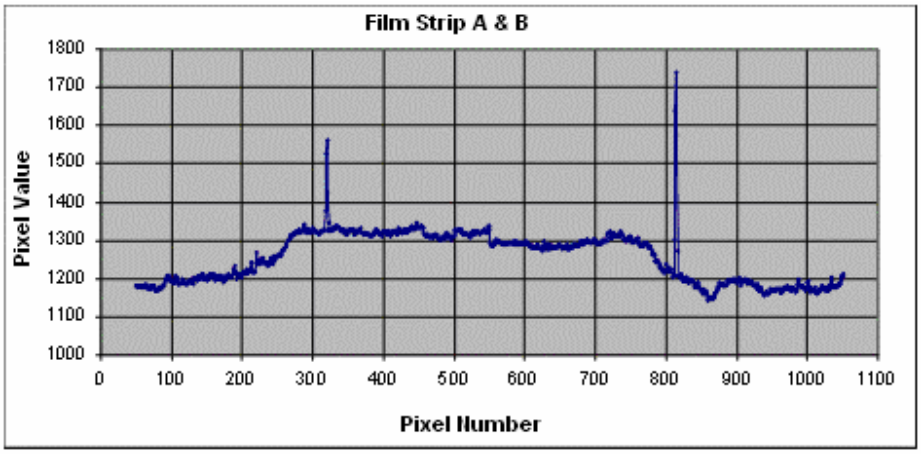

Fig 6.40a). Step position on film strips A & B.

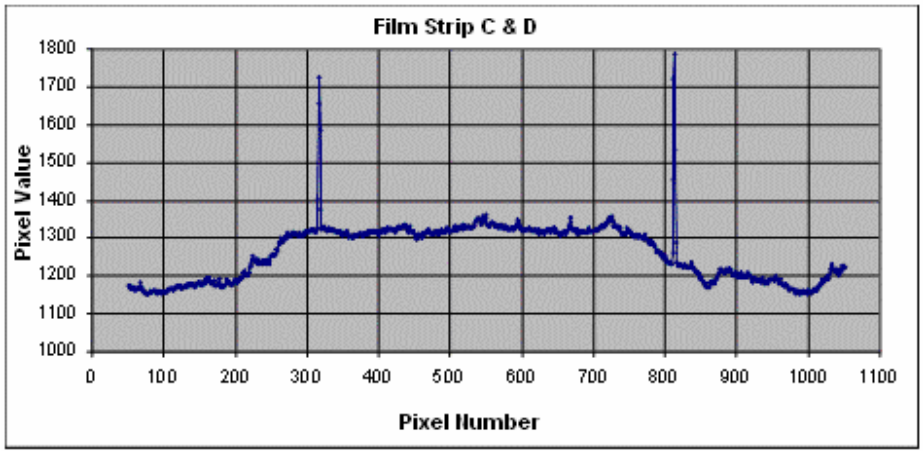

Fig 6.40b). Step position on film strips C & D.

Segment junction determined by the peaks in figures a) and b). The change in pixel value (dose) from segments 1 to 2, and 2 to 3 can be seen as a slope instead of a step.

6.2.12 Dose Step Offset Calculation.

Comparing the peaks to the 50% regions determines how close the DMLC movement was to the segment junctions. To find the offset the distance one pixel represents needs to be calculated.

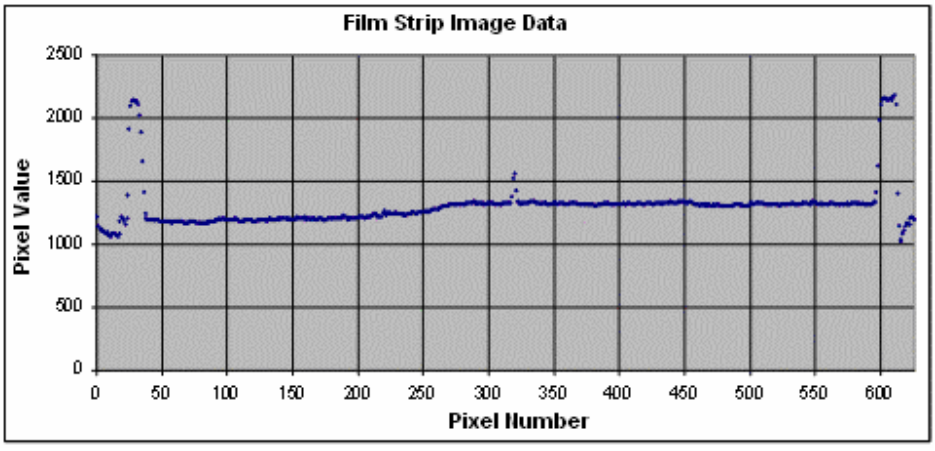

Fig 6.41. Pixel data for Film Strip A, including the pixel values associated with ends of the film strip.

At each end of the profile in Fig. 6.41 there were pixel values which were not associated with the film strip. This data was removed and the number of pixels associated with the film strip could be determined (Fig 6.42).

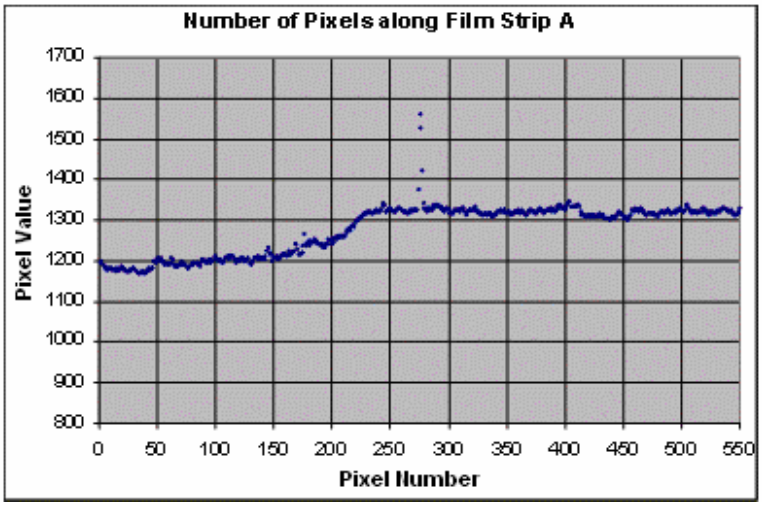

Fig 6.42. Profile of film strip with the excess data removed.

The number of pixels across the film strip was found to be 551pxls.
10cm divided by the number of pixels yields:

1 pixel = 0.018cm.

Peak position:

Pixel number = pixel 276

50% step gradient position:

Fig 6.43 shows the upper and lower plateaus. The upper plateau was approximately 1.000 and the lower plateau was approximately 0.900. Therefore 0.950 was taken to be the 50% of the step gradient. Table 6.14 shows the uncertainties associated with the upper and lower plateau pixel values.

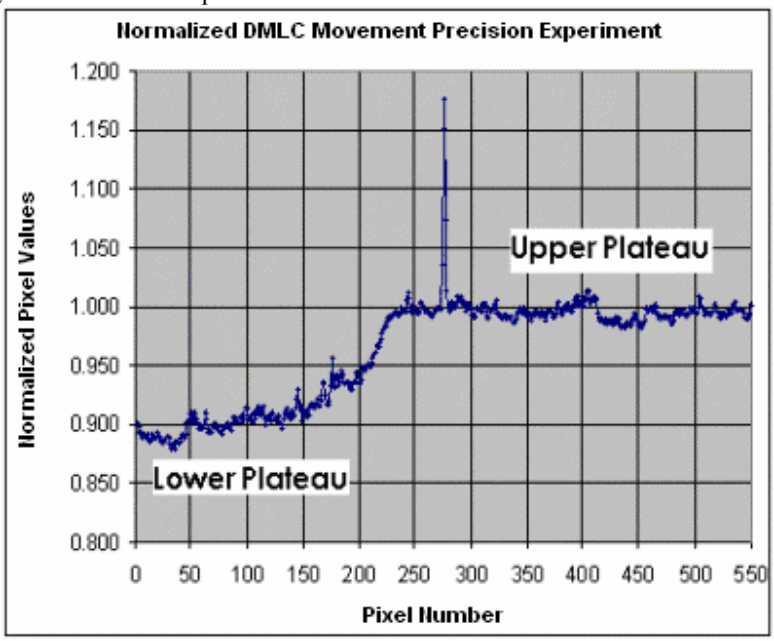

Fig 6.43. The pixel values were normalized to the average pixel value of the step. This shows approximately where the 50% point occurs between the pixel levels.

PLATEAU:	LOWER	UPPER
AVERAGE:	0.900	0.996
STDEV:	0.010	0.006
%ERROR:	1.1%	0.6%

Table 6.14. Average values and uncertainties are shown for the upper and lower plateaus in Fig 6.44.

The position of the 50% was determined to be 206 as shown in Table 8.6.

Position of 50% of Step Gradient	
50% Position	Pixel Number
0.946	203
0.945	204
0.947	205
0.950	206
0.948	207
0.952	208
0.948	209

Table 6.15. Sample of the data from Fig 6.43. At 0.950 the pixel number was 206.

Number of pixels between the peak and 50% of slope = 276-206 = 70pxls.

Distance = 0.018 x 70 = 1.26cm.

The offset of the DMLC movement is approximately 1.3cm.

6.2.13 Physical Scan of Rectangular Phantom.

Nine film squares were irradiated in the scanning physical rectangular phantom and were scanned using the Diagnostic Radiology scanner. The pixel values for the nine film squares were compared to the three film squares used as spot checks for the final calibration curve in. Using the equation obtained from the spot check film the dose to each film square was calculated and is shown in Table 6.16.

FILM #	DISTANCE (cm)	AVERAGE	±(%ERROR)	DOSE (cGy)
1	5	1357.0	0.5%	119.5
2	15	1351.6	0.6%	118.1
3	25	1342.3	0.6%	115.6
4	35	1344.4	0.6%	116.1
5	45	1348.9	0.6%	117.3
6	55	1345.7	0.6%	116.5
7	65	1325.3	0.6%	110.9
8	75	1325.5	0.5%	111.0
9	85	1317.1	0.7%	108.7

Table 6.16. The calculated dose to each film square is shown with the film position and distance in the phantom. Included are the average pixel values for each film square and the associated percent error.

The average dose across the film squares was calculated to be 114.9cGy with a standard deviation of 3.3%. This indicated the slit width of 15.8cm at 100cm SAD was too large and a smaller slit width would be required to deliver 100cGy.

For a relatively small variation in the pixel values there was a large variation in dose. These results indicated that the vidar was not ideal at giving suitable results due to its low sensitivity with Gafchromic-EBT film. An alternative scanner using red light would have greater sensitivity. Precise setup of the rectangular phantom and scanning bed would also help to give satisfactory results.

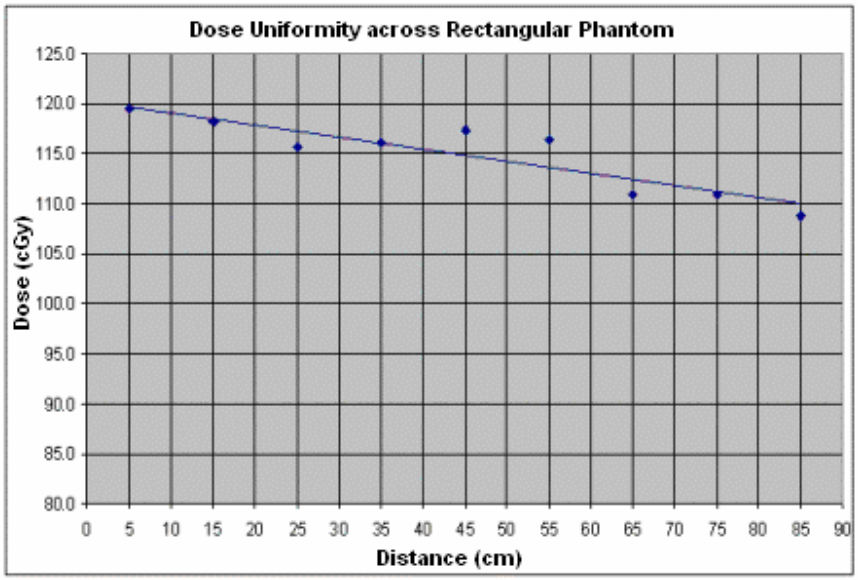

Fig 6.44. Shows the dose variation of the film squares across the rectangular phantom. A linear curve was fitted to guide the eye.

These results were compared to the simulated scan of the rectangular phantom.

6.2.14 Simulated Scan of Rectangular Phantom.

The simulated scan across a rectangular phantom using a slit width of 15.8cm achieved the prescribed dose of 100cGy. The data shown in Fig 6.46 was extended across the rest of the phantom to give a better representation of the dose along the midline of the rectangular phantom. The dose fall-off at each end is not a representation of the dose fall-off due to lack of scattering material. It is due to the limit of applied beams.

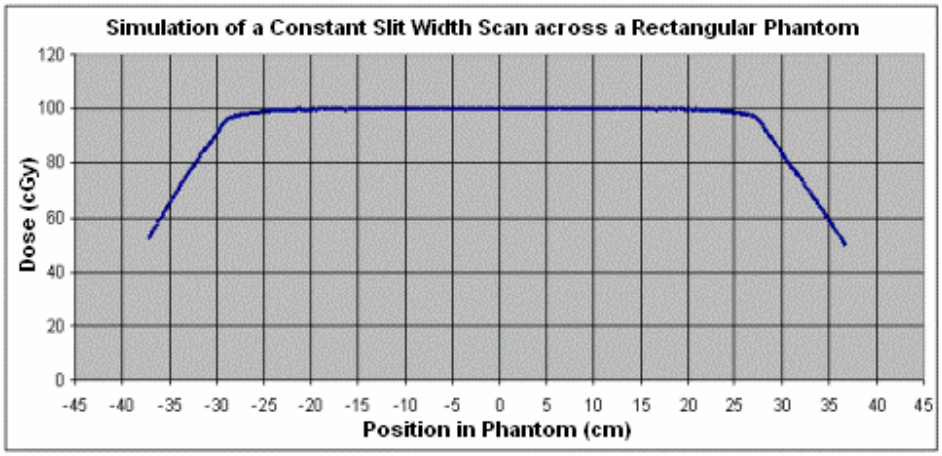

Fig 6.45. Extended dose profile from the simulated constant slit width scan across a simulated rectangular phantom.

This simulation indicated that a slit width of 15.8cm delivered the prescribed dose of 100cGy, while the physical scan did not. From this comparison it was decided that the simulation scan results would be used in the anthropomorphic simulations.

6.2.15 Simulated Constant Slit Width Scan across an Anthropomorphic Phantom.

The slit width used for this scan was determined to be 15.8cm. The delivered dose to the midline for the C_{sw} scan was higher than the prescribed dose of 100cGy over the trunk and neck of the phantom. This indicated that a smaller slit width was required. The dose to the head region, 35 to 45cm, was below 100cGy, which indicated a larger slit width was required. The dose profile in Fig 6.46 shows an inverted image of the phantom surface.

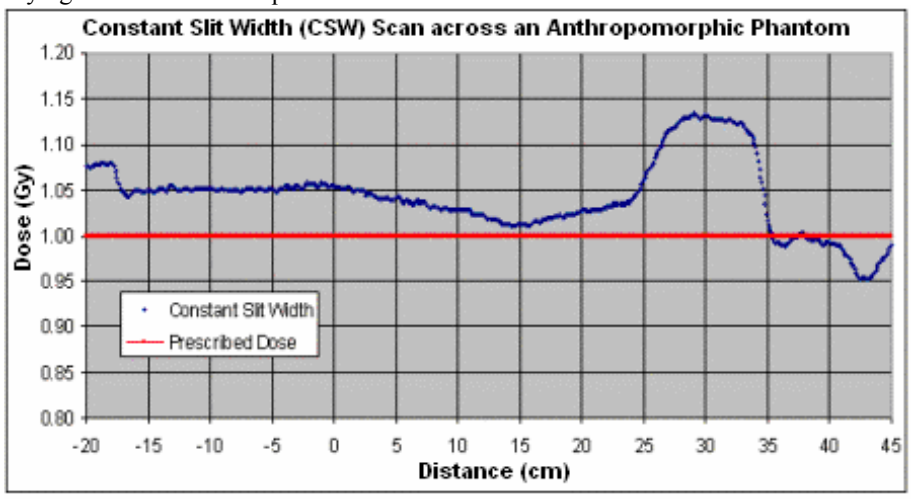

Fig 6.46. Dose profile using the Csw scan across the anthropomorphic phantom.

6.2.16 Simulated Varying Slit Width Scan across an Anthropomorphic Phantom.

To achieve a delivered dose of 100cGy to the midline of the phantom the slit widths were varied. The V_{sw} were calculated from the scanning TMR measurements using the depth to midline data acquired from the Xio software.

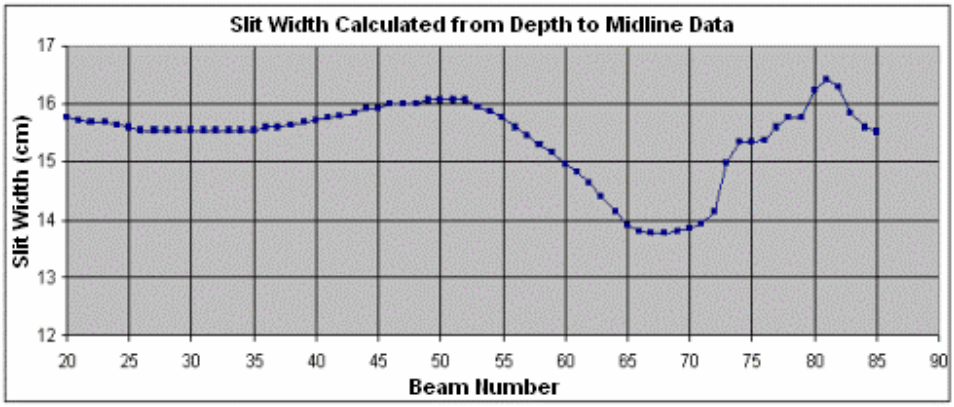

Fig 6.47. Calculated slit widths for each beam.

The calculated slit widths were used to reduce the dose variation along the midline to within ±2.5%. The exception being at the head and neck region, where the dose drops to -3.3%. Each end of the dose profile represents where the beams were outside of the phantom.

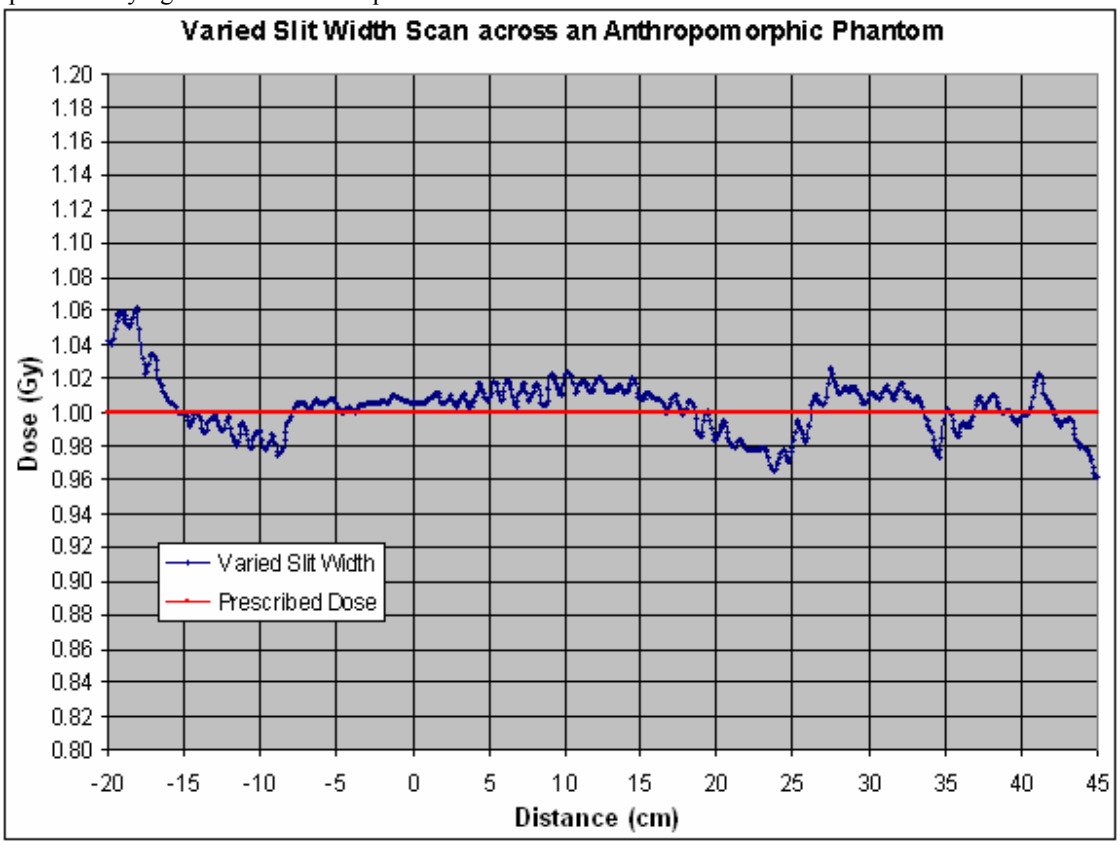

Fig 6.48. Dose profile using a varying slit width technique across an anthropomorphic phantom.

7. FUTURE WORK.

7.1 INTRODUCTION.

The scanning bed system used in this investigation was not a precise system. Leveling and alignment were approximate. Sections 7.3 to 7.6 were initially intended to be investigated. Time constraints limited what could be achieved. The Monte Carlo simulation could not be done as the commissioning of the various Linear Accelerator energies took a longer time than expected. A large amount of time would have been dedicated to the Monte Carlo simulation and would have detracted from the aim of this investigation. Creating limbs for a complete anthropomorphic phantom became a future project because the intended use of the DMLC also became a future project. The DMLC was to be used for modulating the dose to the limbs in an attempt to compensate for the curvature of the limbs.

7.2 SCANNING BED DESIGN.

The setup of the scanning bed needs to be precise. To design a precise scanning bed the areas which need to be addressed would be the i) leveling system, ii) alignment adjustments and iii) a secure flat surface for the phantom. i) Two leveling systems would be required, one for the rails ensuring the scan moves in the plane perpendicular to the collimator axis of rotation, and another for the phantom. The surface the phantom lies on may not be level due to the construction of the bed assembly. A leveling system can ensure the phantom remains at a constant distance from the x-ray focal point. ii) Precise alignment of the scanning bed and phantom ensures the measurements are along the midline of the phantom and not at an angle. A method of aligning the scanning bed system easily would need to be investigated. Using screws at each end of the scanning bed system to finely adjust the position may be one idea. iii) The flat surface for the phantom would be securely attached to the leveling system. Sliding bars which can be clamped around the phantom could be used to keep the phantom in a consistent position over a series of measurements.
This investigation would be done in co-operation with a local engineer or workshop technicians.

7.3 MONTE CARLO SIMULATION.

A Monte Carlo simulation of the scanning bed technique would help determine the dose to the midline of a phantom. Comparisons can then be made between measurements, the TPS calculations and the Monte Carlo calculations. The advantage of the Monte Carlo simulation would be higher degree of accuracy of the dose calculations. The disadvantage would be the time required to do calculations. To simulate this technique a simulated phantom scanning under the beam would need to be designed. The 6MV Linear Accelerator has been designed and commissioned. The next step in this simulation would be to simulate the field size variation as the phantom is scanned.

7.4 COMPLETE ANTHROPOMORPHIC PHANTOM.

The anthropomorphic phantom that was used was not a full body anthropomorphic phantom. In this report calculations were made through the midline of the torso and the head and neck regions. Whereas with the addition of limbs results can be obtained which give an indication as to how well a varying slit width achieves a uniform dose through the limbs. The addition of bolus to the limbs as a way of simplifying the technique can also be investigated. The curvature of the limbs is greater than most regions over the torso. To compensate for this greater curvature the DMLC could be used. Because of this curvature and a constant slit width the limbs receive a larger dose than calculated. Reducing the width of the edges of the field by moving the MLC leaves inwards could compensate for the increased dose as shown in Fig 7.1 below.

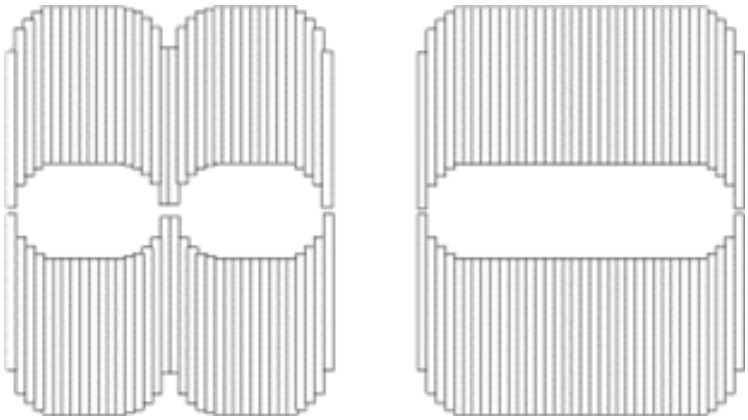

Fig. 7.1. Schematic of DMLC leaf positions compensating for the curvature of the legs. Compensation for between the legs (left). Bolus between the legs simplifies the slit width form (right).

7.5 SHIELDING OF ORGANS AT RISK.

An important part of TBI is the shielding of organs at risk. Certain organs have a greater sensitivity to radiation. If no shielding is used the total dose to the patient is limited by the most radiation sensitive organ, i.e. Lungs. With shielding the total dose to the rest of the body can be increased giving better immunosuppression and a smaller chance of graft versus host disease (GVHD). A variety of techniques for shielding organs at risk exist. With a scanning slit technique shielding can be constructed using partial cerrobend blocks placed on the patient. An alternative technique would be to program the DMLC to reduce the field size over the region of the sensitive organs, similar to compensating for the curvature of the limbs. Specific leaf pairs could move inwards when the sensitive organs are about to move through the beam reducing the dose to that area. This saves on time and materials required to construct blocks.

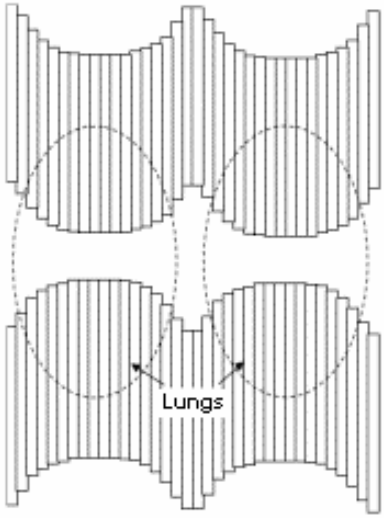

Fig 7.2. Basic schematic of the DMLC shielding lungs.

7.6 DMLC MOVEMENT PRECISION.

In order to achieve precise delivery of dose to specific areas of the phantom the DMLC movement must be precisely matched to the scanning bed movement. Without precise movement dose maxima and minima could occur. Shielding of organs at risk also becomes less effective. A dose maximum occurring within a lung could potentially cause serious side effects. The placement of diodes superiorly and inferiorly to a region could indicate to the DMLC to start moving. Having both systems (DMLC and scanning bed) connected to allow the irradiation and scan to begin simultaneously may also increase the precision of the dose delivery.

8 DISCUSSION.

8.1 INITIAL CONCEPT.

Varying the translating bed speed is one of two possible ways of modulating the radiation beam. The fundamental idea is about varying the exposure time to a point in the patient. This can be done two ways; i) varying the speed the point moves through the beam or ii) vary the field size of the beam which the point is passing through. Advantages of the varying field size technique are that it can be expanded to utilize a Dynamic Multi-Leaf Collimator. Each leaf pair represents a field size which is calculated to deliver the prescribed dose to a point in the patient. The MLC leaves would be orientated in the longitudinal (superior-inferior) direction which allows dose modulation in the transverse direction of the patient, as opposed to dose modulation which is along the longitudinal direction. The DMLC leaves can be used for the shielding of organs at risk, i.e. Lungs and Kidneys. Disadvantages of this technique are; that the planning of such a technique would not be easy or straight forward to implement as each sagittal CT slice associated with a leaf pair must be planned (inverse planning could simplify the procedure). Bolus would be required around the head, feet and between the legs, the patients' head would also need to be fixed in position due to the precision of the treatment. Movement of the head in the longitudinal direction will greatly offset the dose modulation and deliver incorrect doses to the patients' head and neck region.

Developing a system where the DMLC leaf pairs move at the correct time in the treatment would be essential for the precise delivery of the treatment. A feedback system could be used which tells the DMLC software when to move the leaf pairs. This technique requires considerably more research before it can be implemented and is not investigated in this report.

8.2 SUMMARIZED PAPERS.

In this report the technique of using a translating bed with a varying field size for TBI treatment was investigated. A prior paper[11] had investigated the technique of using a translating bed with no form of beam modulation. It was concluded that this technique gave a slightly better dose uniformity compared to the stationary bed technique. They also concluded that varying the bed speed to compensate for the patient thickness yields a greater uniformity through the midline of a patient. Another paper[12] investigated the varying bed speed technique and confirmed a greater uniformity.

8.3 EQUIPMENT.

This investigation concentrated on the field size variation technique. A decommissioned gamma camera bed and rails were acquired from the Nuclear Medicine Department (Christchurch Hospital) to be used as the translating bed in this investigation. The bed top was not a flat level surface and required a board to give the flat level surface. Solid Water blocks were used to make up the rectangular phantom for the initial measurements and were placed on the board on top of the bed. Aligning the Solid Water and the board to the positioning lasers in the treatment room proved to be difficult. Precise alignment of all the equipment was a main issue in this investigation.

The floor of the treatment room was not flat or level. Below the Linac the floor is raised. When setting up the translating bed, the rails are placed first. Each end must be supported to eliminate any bending of the rails and to attempt to create a level platform for the bed. This was difficult as there was no precise way of adjusting the level of the rails or completely eliminating any bending of the rails. With the bed on the rails it was important to ensure that the bed movement would be perpendicular the beam. The positioning lasers were used as a guide. The bed was moved backwards and forwards approximately 1m along the rails to check the alignment. Adjusting the position of the bed was difficult as the rails needed to be moved to move the bed. The Solid Water on the bed top was aligned using the positioning lasers. Source to surface

distance was measured and the bed height adjusted until the SSD was at the required distance. The SSD measurements were done at each end and the middle of the phantom. The SSD measurements varied by ±1mm. It was discovered that the board the Solid Water sits on was slightly bent due to the weight of the Solid Water.

In order to get measurements done the equipment had to be aligned approximately. With the approximate setup of the equipment the initial measurements may not be as precise as desired.

An estimated treatment time for this technique would be approximately 3 minutes for each beam. This time is based on the arbitrarily chosen translating bed speed, though the bed controller computer is capable of moving the bed at a higher speed. The speed is limited by the stepper motor and the pulse rate of the micro processor in the bed controller computer. In the program for the bed controller there is a speed scale where the speed can be adjusted.

8.4 SCANNING TMRS AND SLIT WIDTH DETERMINATION.

Scanning PDD data was acquired but not used in this investigation. The scanning PDD data was to be converted to scanning TMR data but was abandoned. It was simpler to directly measure the scanning TMRs. The scanning TMR measurements were able to determine the effect increasing slit width had on the attenuation of the beam through the phantom, and calculate the slit width required to deliver 100cGy 10cm deep to the midline of the phantom at 120cm SMD. With increasing slit width the TMRs varied little, allowing a constant TMR between varying slit widths. Slit widths could then be calculated using a single equation only dependant on the depth to midline. The calculated slit width was 15.8cm. This slit width was used in a simulation and a physical measurement of a constant slit width scan across a rectangular phantom to test the accuracy of the slit width calculation.

8.5 GAFCHROMIC EBT FILM CALIBRATION.

Dose uniformity and Dynamic MLC movement precision measurements were made using Gafchromic EBT film[18]. The reasons for choosing this type of film were; i) it could cut to any specific size, ii) it could be placed easily between the Solid

Water blocks and iii) it could be used as a dosimeter. Using the film as a dosimeter allowed for the measurement of the dose to the midline of the rectangular phantom which would determine if the calculated slit width was correct. Being Gafchromic film, the film did not need to be developed.

Calibrating the film was a difficult process. The film was cut into 2 x 2cm2 squares and each square irradiated with a different number of Monitor Units (MUs) under reference conditions[15].

Gafchromic EBT film is most sensitive to red light (838nm)[18]. The first film scanner used was a red laser densitometer. It was recommended that a diffusing plate be used with a red laser. A diffusing plate was not readily available and so scans were done without one. The results were noisy and inconsistent with expected results for a film calibration. An X-Rite visual light-point densitometer was used after the red laser densitometer and gave results which were consistent with expected results for a film calibration. The calibration curve was compared to the calibration curve in the product brochure[18]. The calibration curve was of low sensitivity due to the polychromatic light. The X-Rite also had a low measurement resolution of 3 significant figures. A Vidar Scanner was the next scanner to be investigated. This type of scanner also used polychromatic light and yielded a low sensitivity calibration curve. The results however had a greater measurement resolution. Using the Vidar scanner multiple calibration curves were acquired in an attempt to get consistent results. Inconsistencies in the calibration curve measurements were caused by the aging of the film after irradiation. After 2 hours the Gafchromic film has reached 90% of its maximum density growth[18]. A constant time period after irradiation of 1 day was used to make sure the density growth had reached its maximum density growth.

Film orientation was important. The coating direction of the active polymer affected which direction of scanning the film would yield greater sensitivity in the results. This was investigated and the portrait orientation gave less sensitive but consistent results.

Reliable calibration curves were not acquired in this investigation. Using the film as dosimeters was done in the last tests for confirming the calculated slit width delivering 1Gy to the midline 10cm deep at 120cm SMD but did not yield useful results.

8.6 DOSE UNIFORMITY AND DOSE STEP MEASUREMENTS.

The measurements determining the uniformity of dose were done in a rectangular phantom. Gafchromic film was used to measure the dose along the midline and the variation of the pixel values between each film square was within 0.53%. The pixel value variation of each film square was 0.91%.

As discussed in chapter 8 the dose uniformity measurement does not take into account the dose variation in the transverse direction.

The dose step measurements were to determine the precision of the dose step. Film strips 10cm long were placed across a junction of phantom segments. It was observed that the step in dose had a gradient. The 50% of this gradient was used to define the step edge. A line was also drawn across the film strip marking the junction of the segments. The distance between the 50% and this line was calculated to determine the synchrony between the scanning bed system and the DMLC system. The distance was determined to be approximately 1.3cm. This offset could be caused by a difference in time between starting the scan and the irradiation. Scanning a patient would require this offset to be either eliminated or compensated for.

8.7 SIMULATED PHANTOM SCANS USING THE XIO TREATMENT PLANNING SYSTEM.

The comparison between the simulated phantom and the physical phantom showed a distinct difference between the measured doses to midline. The physical scan showed a dose profile which was significantly greater than 100cGy and had a definite gradient which was increasing with the direction of the scan. Whereas the simulated scan gave a dose profile which was at 100cGy and flat along the midline. The results from the physical phantom were found using the Gafchromic film. Calibration of the film was found to be unreliable and therefore determining whether the slit width delivered the correct dose was difficult. Results from the simulated

phantom appeared to be reliable, indicating that the slit width of 15.8cm delivered the correct dose to the midline. This result proved the slit width calculations were correct and could be used for calculating the slit widths which would deliver 100cGy at specific depths to midline.

Depth to midline data was available in a datasheet in the Xio planning system. Using the depth data a range of slit widths compensating for these depths were calculated. Beams were then applied using the calculated slit widths. In order to simulate the scan accurately each point along the midline had to see the correct slit width. With the application of 90 beams this procedure took a large amount of time complete. To simplify the application of the beams the anthropomorphic phantom was separated into segments which defined simpler shapes. Curves were approximated as flat lines, sloped lines or steps. This method was subjective in determining where the phantom was segmented. Adjusting the slit widths between the beams required using asymmetrical jaws. The change in off-axis factor in this direction would cause dose variation along the midline. The off-axis factor was not taken into account in this simulation. The Xio treatment planning system made the dose calculations for the 90 beams. The dose calculations for 90 beams required 30 minutes to be completed. A dose profile was taken along the midline of the phantom showing the variation along the midline to be within 2.5%, where the head and neck region had the greatest dose variation of approximately -3.3%. The beginning of the profile shows where the beams started outside the phantom. Planning a varying slit technique for a patient in a reasonable period of time would not be plausible. The beam limit also makes the procedure difficult.

9 CONCLUSION.

The theory and literature demonstrated that greater dose uniformity was achievable with a scanning bed technique in comparison to a static field technique. From this investigation dose uniformity to within ±1%in a rectangular phantom was achieved. Difficulties arose with calculating the appropriate slit width which could achieve a prescribed dose of 100cGy to the midline. The dose uniformity across the head and neck region of the anthropomorphic phantom was a complex and time consuming process. Precise setup of the equipment used in the scanning TMR and slit width measurements was difficult to accomplish and may be a cause for the inaccuracies in the calculations of the slit width. Simulations using the calculated slit widths produced a dose uniformity along the midline to within ±2.5% (exception being -3.3% over the head and neck region). Planning a treatment for this technique would be a long process and would require a large period of time for a single patient. The beam limit in the Xio treatment planning system makes applying beams over an entire patient difficult. A way around this would be to increase the slit width and reduce the scan speed. Less beams would be required allowing for a greater beam coverage. This investigation has shown that varying the field size as a phantom scans under the beam can compensate for depth to midline variations and produce a uniform dose to within ±2.5%.

10. REFERENCES.

1. J. Van Dyk, J.M. Galvin, G. P.Glasgow, E. B. Podgorsak. *"The Physical Aspects of Total and Half Body Photon Irradiation."* A Report of Task Group 29 Radiation Therapy Committee American Association of Physics in Medicine, AAPM Report 17: 20, 21.1986.

2. Based on presentation by Colleen Lawton. *"Total Body Irradiation for Bone Marrow Transplantation."* Oncology 13: 1-9, 1999.

3. J. Van Dyk. *"Dosimetry for Total Body Irradiation."* Radiotherapy and Oncology: 107-118. 1987.

4. Mahmut Ozsahin, Yazid Belkacemi, Francoise Pene, et al. *"Total-Body Irradiation and Cataract Incidence: A Randomized Comparison of Two Instantaneous Dose Rates."* Int. J. Rad. Onc. Biol. Phys. 28: 343-347. 1993.

5. Inoue T, Ikeda H, Yamazaki H, Tang J T, Song C, Teshima T, Murayama S, Ohtani M, Shibata H, Masaoka T. *"Role of Total Body Irradiation as Based on the Comparison of Preparation Regimens for Allogeneic Bone Marrow Transplantation for Acute Leukemia in First Complete Remission."* Strahlenther Onkol. 169: 250-5. April 1993.

6. Frederick R. Appelbaum. *"The Influence of Total Dose , Fractionation, Dose Rate, and Distribution of Total Body Irradiation on Bone Marrow Transplantnation."* Seminars in Oncology 20 (Suppl 4): 3-10, 1993.

7. Mahmut Ozsahin, Francoise Pene, Emmanuel Touboul, et al. *"Total-Body Irradiation Before Bone Marrow Transplantation."* Cancer 69: 2853-2865, 1992.

8. Renzo Corvo, Gabriella Paoli, Salvina Barra, et al. *"Total Body Irradiation Correlates with Chronic graft Versus Host Disease and Affects Prognosis of Patients*

with Acute Lymphoblastic Leukemia Receiving an HLA Identical Allogeneic Bone Marrow Transplant." Int. J. Rad. Onc. Biol. Phys. 43: 497-503, 1999.

9. International Commission on Radiation Units and Measurements (ICRU). *Determination of Absorbed Dose in a Patient Irradiated by Beams of X or Gamma Rays in Radiotherapy Procedures.* ICRU Report 24: 4-8. 1976.

10. Wen-Long Hsieh. *Total Body Irradiation on an Isocentric Linear Accelerator: A Dynamically Sweeping Beam Technique.* Arc-TBI. 2003.

11. Mehrdad Sarfaraz, Cedric Yu, D. J. Chen, and Leon Der. *"A translational couch technique for total body irradiation."* Journal of Applied Clinical Medical Physics 4: 201-209. 2001.

12. Mario Chre´ tien, Carl Coˆ te´ , Roger Blais, Lucie Brouard, Lise Roy-Lacroix, and Marie Larochelle. *"A variable speed translating couch technique for total body irradiation."* Med. Phys. 27: 1127-1130. May 2000.

13. L. H. Gerig, J. Szanto, T. Bichay, and P. Genest, *"A Translating-Bed Technique for Total-Body Irradiation."* Phys. Med. Biol 39: 19-35. 1994.

14. Varian Medical Systems. *"DMLC: Implenemntation Guide."*

15. Pedro Andreo, David T Burns, Klaus Hohlfeld, M Saiful Huq, Tatsuaki Kanai, Fedele Laitano, Vere Smyth, Stefaan Vynckier. *"Absorbed Dose determination in External Beam Radiotherapy: An International Code of Practice for Dosimetry based on Standards of Absorbed Dose to Water."* IAEA TRS-398. 21 May, 2001.

16. British Institute of Radiology and the Institution of Physics and Engineering in Medicine and Biology. *"Central Axis Depth Dose Data for Use in Radiotherapy: 1996".* BJR Supplement 25: 153-157, 1996.

17. Ervin B. Podgorsak et al. *"Review of Radiation Oncology Physics: A Handbook for Teachers and Students."* Educational Report Series: 422-426, 2003.

18. *"Gafchromic® EBT Self-Developing Film For Radiotherapy Dosimetry."* International Specialty Products. 2005. www.ispcorp.com/products/dosimetry/content/brochures/

19. Xio Online Help, Index, Beam Overview.

APPENDIX.

Scanning Couch Program.

```
DECLARE SUB motion ()
' common variables
COMMON SHARED topspeed!, dir!, posn!, estop, steps

' subroutines
DECLARE SUB a1 ()
DECLARE SUB d1 ()
DECLARE SUB move (td!)

' set some defaults.
dir = 223
topspeed = 20
mm = 1

' print instructions and input command
DO WHILE cmd$ <> "e"
        estop = 0
        CLS
        PRINT "Stepper control unit Mk I"
        PRINT : PRINT "Commands :"
        PRINT "fx - move forward x steps"
        PRINT "fxk - move forward x thousand steps"
        PRINT "fxM - move forward x million steps"
        PRINT "bx - move backward x steps"
        PRINT "m - set millimeters mode for positions and movements"
        PRINT "p - set pulses mode for positions and movements"
        PRINT "r - reset position counter"
        PRINT "sx - set the slowness factor to x"
        PRINT "e - exit programme"
        PRINT
' print current settings.
        IF mm = 0 THEN
                PRINT "Current position = "; posn; "pulse",
        ELSE
                PRINT "Current position = "; posn / 480; "mm",
        END IF
        PRINT , "Slowness = "; topspeed
        INPUT "instructions please"; instruction$
' parse command
        cmd$ = LEFT$(instruction$, 1)
        instlen = LEN(instruction$)
        operand$ = MID$(instruction$, 2, instlen - 1)
        mult$ = RIGHT$(operand$, 1)
        IF mult$ = "k" THEN
                nums = VAL(MID$(operand$, 1, instlen - 2)) * 1000
        ELSE
                IF mult$ = "M" THEN
                        nums = VAL(MID$(operand$, 1, instlen - 2)) *
1000000
                ELSE
                        nums = VAL(MID$(operand$, 1, instlen - 1))
                END IF
        END IF
' selectivly execute command.
' scale = mm OR pulses
        IF cmd$ = "m" THEN mm = 1
```

```
        IF cmd$ = "p" THEN mm = 0

' forward move
        IF cmd$ = "f" THEN
                dir = 223
                IF mm = 1 THEN
                        PRINT "Moving forward "; nums; " mm"
                        nums = nums * 480
                ELSE
                        PRINT "Moving forward "; nums; " steps"
                END IF
                steps = nums
                CALL motion
        END IF

' move backward (Identical to forward except for direction)
        IF cmd$ = "b" THEN
                dir = 191
                IF mm = 1 THEN
                        PRINT "Moving backward "; nums; " mm"
                        nums = nums * 480
                ELSE
                        PRINT "Moving backward "; nums; " steps"
                END IF
                steps = nums
                CALL motion
        END IF

' Change settings
        IF cmd$ = "r" THEN posn = 0
        IF cmd$ = "s" THEN topspeed = nums
LOOP
STOP

SUB a1
'       Accelerate. Give a pulse with a long time delay, then give
another
'       pulse with a shorter time delay, etc, until topspeed is
reached.

a = 20
DO WHILE a > 1
        a = a / 1.001
        b = topspeed * a
        CALL move(b)
LOOP
END SUB

SUB d1
'       decelerate movement. Give a pulse then vary the time delay
'       before the next pulse.

a = 20
DO WHILE a > 1
        a = a / 1.001
        b = topspeed * (20 / a)
        CALL move(b)
LOOP
END SUB

SUB motion
```

```
'       Overall motion control, supervises movements

' move short distance slowly
        IF steps < 5996 THEN
                FOR a = 1 TO steps
                        IF estop = 1 THEN EXIT FOR ' estop - just
stop
                        CALL move(1000)
                NEXT
        ELSE

' move others by accelerating, moving fast & decellerating
                steps = steps - 5996
                CALL a1
                FOR a = 1 TO steps
                        IF estop = 1 THEN EXIT FOR ' estop - decel
now
                        CALL move(topspeed)
                NEXT
skip1:          CALL d1

        END IF

END SUB

SUB move (td)
'       Generate a negative going pulse on only one data line of
'       the printer port. (given by 'dir'). Then wait td (time delay)
'       counts before returning

'       Keep track of actual position by either incrementing
'       OR decrementing pulse count.

' Check for emergency stop !
IF INKEY$ <> "" THEN estop = 1
IF dir = 223 THEN
        posn = posn + 1
ELSE
        posn = posn - 1
END IF
OUT &H378, dir
OUT &H378, 255
FOR w = 1 TO td
NEXT w
END SUB
```